

1 **Title: AAV-delivery of diacylglycerol kinase kappa achieves long-term**
2 **rescue of *Fmr1*-KO mouse model deficits of fragile X syndrome**

3
4 **Authors:** Karima Habbas¹, Oktay Cakil^{1†}, Boglarka Zambo^{1†}, Ricardos Tabet^{1‡}, Fabrice
5 Riet², Doulaye Dembele¹, Jean-Louis Mandel¹, Michaël Hocquemiller³, Ralph Laufer³,
6 Françoise Piguet⁴, Hervé Moine^{1*}

7
8 **Affiliations:**

9 ¹Institut de Génétique et de Biologie Moléculaire et Cellulaire (IGBMC), Département de
10 Médecine Translationnelle et Neurogénétique, Centre National de la Recherche Scientifique
11 (CNRS UMR7104), Institut National de la Santé et de la Recherche Médicale (INSERM
12 U1258), Université de Strasbourg, Illkirch, France.

13 ²Institut de Génétique et de Biologie Moléculaire et Cellulaire (IGBMC), PHENOMIN-ICS,
14 Centre National de la Recherche Scientifique (CNRS UMR7104), Institut National de la
15 Santé et de la Recherche Médicale (INSERM U1258), Université de Strasbourg, Illkirch,
16 France

17 ³Lysogene, Neuilly-sur-Seine, France.

18 ⁴NeuroGenCell, INSERM U1127, Paris Brain Institute (ICM), Sorbonne University, CNRS,
19 AP-HP, University Hospital Pitié-Salpêtrière, Paris, France.

20
21 *Corresponding author. Email: moine@igbmc.fr

22 † equal contribution

23 ‡ Present address: Pfizer, Inc, Cambridge, MA, USA.

24
25 **One sentence summary:** *DGKk* gene therapy in *Fmr1*-KO mouse model

26
27 **Keywords:**

28 Fragile X syndrome, FMRP, AAV, diacylglycerol kinase, *Fmr1*-KO

29
30 **Contact:**

31 Hervé Moine, Institut de Génétique et Biologie Moléculaire et Cellulaire (IGBMC), 67404
32 Illkirch, France, Phone +33 3 88 65 56 78, Email: moine@igbmc.fr

33

34

35 **Abstract:**

36 Fragile X syndrome (FXS) is the most frequent form of familial intellectual disability. It
37 results from the lack of the RNA binding protein FMRP and is associated with the
38 overactivation of signaling pathways downstream of mGluRI receptors and upstream of
39 mRNA translation. We previously found that diacylglycerol kinase kappa (DGKk) is a main
40 mRNA target of FMRP in cortical neurons. Here we show that diacylglycerol kinase kappa
41 (DGKk), when modified as to become FMRP-independent and delivered into the brain of
42 adolescent mice using adeno-associated viral vectors, corrects brain diacylglycerol and
43 phosphatidic acid homeostasis and the main phenotypic behaviors of the *Fmr1*-KO mouse
44 model of FXS. Thus, DGKk appears as a key triggering factor of FXS pathomechanism while
45 providing a possible means of intervention for FXS gene therapy.

46

47 **Main Text:**

48

49 **INTRODUCTION**

50 Fragile X syndrome (FXS) is a main cause of familial intellectual disability and autistic
51 spectrum disorder (ASD) with a prevalence in general population estimated as 1 in 5000
52 males and 1 in 8000 females (Hagerman et al., 2017; Kaufmann et al., 2004). FXS is also
53 generally associated with variable behavioral symptoms that can include anxiety,
54 hyperactivity, hypersensitivity, stereotypies, memory deficits and sleeping problems. FXS
55 results from the loss of the fragile X mental retardation protein (FMRP), an RNA binding
56 protein associated to mRNAs and the translation machinery and whose absence in *Fmr1*-
57 deleted mice (*Fmr1*-KO) recapitulates FXS-like phenotypes (1994; Mientjes et al., 2006),
58 with perturbation of neuronal protein translation in hippocampus and cortex (Dolen et al.,
59 2007; Qin et al., 2005). FMRP loss leads to mRNA translation increase of neuronal proteins
60 resulting from an overactivation of metabotropic group 1 glutamate receptor (mGluR)-
61 dependent local mRNA translation (Bear et al., 2004), including phosphatidylinositol 3-kinase
62 enhancer (PIKE) (Gross et al., 2015), matrix metalloproteinase 9 (MMP9) (Gkogkas et al.,
63 2014; Sidhu et al., 2014), glycogen synthase kinase 3 (GSK3) (Guo et al., 2012) and amyloid-
64 β A4 protein (APP) (Pasciuto et al., 2015; Westmark et al., 2011). The mGluR overactivation
65 is one well established triggering factor of FXS pathomechanism, and we recently showed
66 that mGluR diacylglycerol (DAG) and phosphatidic (PA) dependent signaling upstream of
67 local mRNA translation is disrupted by FMRP loss (Tabet et al., 2016a). The diacylglycerol

68 kinase kappa (DGKk) transcript was identified in mouse cortical neurons as the mRNA
69 species most bound by FMRP and with highest in vitro binding affinity. DGKk expression
70 was found severely reduced in the brain of *Fmr1*-KO mouse and a perturbation of DAG/PA
71 acid homeostasis was observed in *Fmr1*-KO cortical neurons and in the brain of FXS
72 individuals, suggestive of a decreased DGK activity and altered DAG/PA signaling (Tabet et
73 al., 2016a). DGKk knockdown in wild-type mouse brains recapitulated FXS-like behaviors,
74 and overexpression of DGKk in *Fmr1*-KO hippocampal slices rescued their abnormal
75 dendritic spine morphology (Tabet et al., 2016a). Overall, DGKk appears to play a key role in
76 dendritic spine morphology and function and in the determination of FXS-like behaviors.
77 DGKk loss of function was proposed to be at the origin of the various forms of abnormal
78 synaptic signaling in FXS by causing altered DAG/PA signaling (Tabet et al., 2016b). Thus,
79 being the most proximal downstream mediator of FMRP action, DGKk could represent an
80 interesting actionable therapeutic target.

81 Here we show that DGKk expression is lost in FXS patients' postmortem brains as previously
82 shown in *Fmr1*-KO mice (Tabet et al., 2016a). We show that the N-terminal region of DGKk
83 is important for its positive translational control by FMRP and the deletion of this region
84 renders the protein (Δ N-DGKk) independent of FMRP, suggesting that FMRP alleviates a
85 translation blockade within the N-terminal region. Δ N-DGKk is able to modulate protein
86 synthesis rate and eIF4E phosphorylation in neurons. Moreover, Δ N-DGKk expression in
87 *Fmr1*-KO mouse brain using adeno-associated virus Rh10 (AAVRh10) is able to correct brain
88 lipid profile dysregulations and achieve long term behavioral rescue (over 8 weeks after
89 injections) of *Fmr1*-KO mouse, providing a first proof of principle of *DGKk* gene therapy in a
90 mouse model of FXS.

91

92 **RESULTS**

93

94 **DGKk mRNA translation requires FMRP and DGKk N-terminal truncation alleviates** 95 **FMRP control.**

96 We previously showed that the expression of diacylglycerol kinase kappa (DGKk) is strongly
97 reduced in brain of *Fmr1*-KO mouse (Tabet et al., 2016a) in agreement with the fact that
98 DGKk mRNA was identified as the most abundant mRNA species associated with FMRP by
99 crosslinking immunoprecipitation in cortical neurons, and with the highest in vitro binding
100 affinity. Like in *Fmr1*-KO mouse brain, DGKk expression is also lost in FXS post-mortem
101 cerebellum compared to unaffected controls (**Fig. 1A**). These data suggest that DGKk

102 requires FMRP for its proper expression. DGKk is mostly expressed in neurons and is almost
103 absent in non-neuronal cells (Tabet et al., 2016a). We then tested if it is possible to
104 recapitulate FMRP control in a non-neuronal cell system. We analyzed the influence of
105 FMRP on the expression of HA-tagged mouse and human DGKk (**Fig. 1B, Sup Fig. 1A**)
106 transfected into two different cell lines, Cos-1 and HeLa. Knock-down of endogenous FMRP
107 with siRNA severely reduced the expression level of mouse DGKk (mDGKk) compared to
108 control siRNA treated Cos-1 cells (**Fig. 1BC**) indicating a strong FMRP requirement for
109 DGKk expression. Human DGKk (hDGKk) level is also affected by FMRP knock-down,
110 indicating that FMRP control is conserved on RNA sequences from different species (**Sup**
111 **Fig. 1A**). mDGKk mRNA level is not influenced by the lack of FMRP (**Sup Fig. 1B**), while
112 the protein level is severely reduced, supporting a control mechanism at the mRNA
113 translational level. This is in agreement with our previous data in mouse brain indicating that
114 DGKk transcript level is not affected by the loss of FMRP, and DGKk mRNA is less
115 associated with polyribosomes (Tabet et al., 2016a). Noticeably, DGKk is the only DGK
116 isozyme interacting strongly with FMRP (Tabet et al., 2016a) and bearing a long N-terminal
117 extension constituted of unique proline-rich and EPAP repeated motives (Imai et al., 2005)
118 (**Fig. 1B**). The N-terminal part of the protein might play a critical role in DGKk expression
119 considering the repetitive nature of the EPAP domain at the beginning of the coding
120 sequence. Thus, we generated a mDGKk construct lacking the first 696 bases following the
121 start codon, encompassing the EPAP domain (Δ N-DGKk), for expression assessment in cells.
122 Δ N-DGKk lead to a strong increase of expression (about ten-fold higher) (**Fig. 1D**). FMRP
123 reduction did not affect Δ N-DGKk (**Fig. 1D**), suggesting that the N-terminal domain of
124 DGKk is required for FMRP control and that Δ N-DGKk expression does no longer depend on
125 the presence of FMRP. Therefore, Δ N-DGKk represents a potential therapeutic target for FXS
126 gene therapy by bypassing the need for FMRP.

127

128 **Δ N-DGKk counteracts with FXS-like molecular defects.**

129 DGKk deregulation has been proposed to play a key role in FXS pathomechanism by altering
130 DAG/PA signaling and leading to an excess of DAG and lack of PA potentially responsible of
131 excessive protein synthesis, the major molecular hallmark of FMRP defects (Tabet et al.,
132 2016a; Tabet et al., 2016b). To test the potential rescuing activity of Δ N-DGKk, we first
133 analyzed its ability to modulate protein synthesis rate. Expression of Δ N-DGKk in Cos-1 cells
134 reduced in a concentration dependent manner the protein translation rate, and this effect was
135 counteracted by pretreatment of cells with DGK specific inhibitors R59022 and R59949

136 (Jiang et al., 2000) (**Fig. 2A**). These data demonstrate that Δ N-DGKk activity is upstream of
137 mRNA translation and relies on conversion of DAG into PA, as DGK inhibitors prevent Δ N-
138 mDGKk from reducing mRNA translation by blocking its enzymatic activity.
139 To assess the biodistribution and efficacy of Δ N-DGKk in a FXS mouse model, we built our
140 expression cassette to be driven by the neuron specific promoter synapsin and packaged into
141 two different adeno-associated viral vectors (AAV), Rh10 and PHP.eB. Both AAV vectors
142 harboring Δ N-DGKk demonstrated efficient neuronal transduction in *Fmr1*-KO cortical
143 neurons, confirming that Δ N-DGKk can be expressed in the absence of FMRP (**Fig. 2B**).
144 Phosphorylation of initiation factor eIF4E, which regulates protein synthesis by reducing
145 translation initiation level (Sonenberg, 1994) and is increased after DAG-signaling activation
146 (Wang et al., 1998), is increased in *Fmr1*-KO mouse and FXS patients (Gantois et al., 2017).
147 We show that P-eIF4E is also increased in *Fmr1*-KO mouse cortical neurons compared to WT
148 littermates (**Sup Fig. 2A**) and Δ N-DGKk is able to reduce their eIF4E phosphorylation (**Fig.**
149 **2C**). No sign of Δ N-DGKk-specific neuronal toxicity was observed in neuronal cultures
150 transduced with AAV expressing Δ N-DGKk at high multiplicity of infection (MOI) (**Sup Fig.**
151 **2B-E**). An overall reduction in NeuN positive cells was observed upon treatment of cells with
152 AAV, independently from Δ N-DGKk expression, as the same effect was observed with AAV-
153 FMRP. Such effect was visible with a 10-fold lower amount of AAV-FMRP (10e9 VG/well)
154 (**Sup Fig. 2D**). Additional tests (caspase 3/7, LDH) did not show signs of toxicity in vitro
155 (**Sup Fig. 2B, C**).

156

157 **In vivo correction of phosphatidic acid level in adult mice using multiple routes of** 158 **administration**

159 Δ N-DGKk was administered to 5-week-old *Fmr1*-KO mice by intravenous injection of
160 AAVPHP.eB- Δ N-DGKk or intracerebral injection into the striatum and hippocampus of
161 AAVRh10- Δ N-DGKk, respectively. Single retro-orbital injection of AAVPHP.eB- Δ N-DGKk
162 at 10^{11} VG/mouse enabled 0.5-1 VG/cell throughout the brain (**Fig. 3AB**) four or eight
163 weeks after injection, with low protein expression as visualized by Western blot (**Fig. 3C**) and
164 immunohistochemistry (**Fig. 3D, Sup Fig. 3A**). Intracerebral injection of AAVRh10- Δ N-
165 DGKk at 5×10^{11} VG/mouse enabled higher brain transduction, with about 100 VG/cell in
166 the hippocampus and about 25 VG/cell in rest of brain leading to high protein expression
167 levels (**Fig. 3BCD**). AAVRh10 vector lead to robust Δ N-DGKk expression throughout the
168 hippocampus (CA1 and CA2 regions mainly), cortex and striatum (**Fig. 3D, Sup Fig. 3A**).

169 DGKk deregulation was shown to alter DAG/PA balance in neuronal cultures and human
170 postmortem brains (Tabet et al., 2016a). We confirmed a marked decrease of total PA level
171 (22% ±8) in the cortex of *Fmr1*-KO mice at 13 weeks of age (**Fig. 3E**). The other mouse brain
172 regions did not show significant differences (**Sup Fig. 3B**). The decrease in the total pool of
173 PA is reflected by a reduction of most PA species (including abundant species 34:1, 36:2,
174 38:4 or low species 38:3, 40:1) (**Sup Fig. 3D-F**). Thus, DGKk loss in *Fmr1*-KO cortex led to
175 alteration of PA phosphorylation independent from fatty acid patterns. ΔN-DGKk delivery to
176 the brain alleviated PA reduction in *Fmr1*-KO and led to a PA level comparable to vehicle
177 injected WT mice (**Fig. 3E**). This is true for all fatty acid PAs with levels undistinguishable
178 from control, demonstrating a complete rescue of PA by ΔN-DGKk expression (**Sup Fig. 3D-**
179 **F**). Intravenous delivery of PHP.eB-ΔN-DGKk led to partial correction of total PA level (**Fig.**
180 **3E**) that was further confirmed at the single PA level, indicating that ΔN-DGKk is able to
181 balance the PA with only few neurons transduced (**Sup Fig. 3D-F**). Total DAG level was not
182 significantly altered in cortex (**Fig. 3F**) and other brain areas tested (**Sup Fig. 3C**), and at the
183 level of individual DAG species (**Sup Fig. 3 G-I**). Nine other lipid classes tested did not show
184 significant differences between the groups (**Sup Fig. 7J**) indicating that the effect of ΔN-
185 DGKk is restricted to the correction of DAG/PA balance.

186 187 **AAVRh10-ΔN-DGKk achieves long-term rescue of *Fmr1*-KO behavioral defects.**

188 Four weeks after injections, a battery of behavioral tests was performed on the AAV injected
189 *Fmr1*-KO mice and their vehicle injected WT (WT-S) or *Fmr1*-KO (Fmr1-S) littermate
190 controls (**Sup table 1**). Vehicle injected *Fmr1*-KO mice showed an increase of time spent and
191 in number of entries in open arms of the elevated plus maze (EPM) compared to the WT-
192 vehicle mice (1.9 and 1.8-fold of mean increase, respectively), suggesting decreased anxiety
193 induced by the genotype. In contrast, AAVRh10-ΔN-DGKk treated mice (Fmr1-Rh10)
194 showed no difference compared to WT-vehicle mice (**Fig. 4A**). A similar phenotype was
195 observed in the open field arena of novel object recognition test (NOR), where vehicle
196 injected *Fmr1*-KO mice showed an increase of time spent in the center of the arena, while
197 AAVRh10-ΔN-DGKk treated mice were not different from WT-vehicle (**Fig. 4B**).
198 Vehicle injected *Fmr1*-KO mice showed increased locomotor activity compared to WT-
199 vehicle mice. This phenotype was seen in the EPM test (**Fig. 4A**, number of entries in open
200 and closed arms), in the open field arena of NOR (**Fig. 4B**, distance travelled in habituation,
201 acquisition and retention phases) and in the habituation phase of three-chambers social
202 recognition test (**Fig. 4C**, number of entries), and was corrected in all tests with AAVRh10-

203 Δ N-DGKk treatment. Signs of hyperactivity of *Fmr1*-KO mice were also seen in the first hour
204 of light and dark phases of actimetry test (**Sup Fig. 4AB**), suggesting this phenotype is related
205 to novelty of environment. AAVRh10- Δ N-DGKk treated mice did not show this phenotype.
206 No difference in recognition index was observed between genotypes in the NOR test (**Fig.**
207 **4B**). Performing the NOR test in a smaller size arena ameliorated the recognition index of
208 objects (**Sup Fig. 4D**), in correlation with longer object exploration times of objects (**Sup Fig.**
209 **4CD**, explorations). However, no difference was observed between the genotypes, suggesting
210 an apparent lack of significant memory impairment of the *Fmr1*-KO mice. In small size arena
211 the hyperlocomotor activity phenotype of *Fmr1*-KO mice was not visible (**Sup Fig. 4D**),
212 potentially because this environment was less anxiogenic than a larger arena. *Fmr1*-KO
213 vehicle mice showed a trend to dig more, to bury more marbles and to spend less time in
214 grooming compared to the WT-vehicle mice, but these differences were not statistically
215 significant (**Sup Fig. 4E**). Δ N-DGKk treatment seemed to counteract these effects, but the
216 high variability of these phenotypes between mice precluded drawing conclusions.
217 Vehicle injected *Fmr1*-KO mice showed an increased number of entries in the three-chambers
218 social recognition test and this phenotype was corrected with AAVRh10- Δ N-DGKk (**Fig. 4C**,
219 **Sup Fig. 4F**). For social preference over object, no difference was observed between
220 genotype groups (**Fig. 4C**, **Sup Fig. 4F**) indicating there was no significant effect of mutation
221 or treatment on social preference. In the social memory test, *Fmr1*-KO mice failed to
222 recognize previously encountered mice, while *Fmr1*-KO mice treated with AAVRh10- Δ N-
223 DGKk had a higher recognition index relative to untreated mice (**Fig. 4C**).
224 Vehicle injected *Fmr1*-KO mice also showed a reduced ability to build a nest after 5 and 24h.
225 AAVRh10- Δ N-DGKk treatment rescued this phenotype (**Sup Fig. 4G**).
226 The phenotypes observed at 4 weeks after injections were generally recapitulated in older
227 animals at 8 weeks after injection (**Sup Fig. 5A-F**). Consistent with the stability of the
228 treatment effect, no significant variation of Δ N-DGKk protein level was observed between 8
229 and 12 weeks after AAV injection (corresponding to animal groups phenotyped at 4 and 8
230 weeks, respectively) (**Sup Fig. 3A**). *Fmr1*-KO-vehicle mice tested at 8 weeks showed
231 reduced recognition index in NOR test compared to WT-vehicle and *Fmr1*-KO-Rh10- Δ N-
232 DGKk (**Sup Fig. 5D**), but within a smaller test arena where *Fmr1*-KO-vehicle mice exhibit
233 less hyperactivity (**Sup Fig. 5E**) all groups performed equally, suggesting that the memory
234 performance alteration of *Fmr1*-KO mice might be caused by hyperactivity. *Fmr1*-KO-
235 vehicle mice tested at 8 weeks after injection (13-week-old) showed a strong digging behavior
236 compared to WT-vehicle and *Fmr1*-KO-Rh10- Δ N-DGKk, a phenotype that was not visible at

237 4 weeks (**Sup Fig. 5F**). An increase in body weight was observed in *Fmr1*-KO-vehicle group
238 compared to WT-vehicle. WT-vehicle and *Fmr1*-KO-Rh10- Δ N-DGKk showed no weight
239 difference, suggesting the treatment rescued this phenotype (**Sup Fig. 5G**).
240 *Fmr1*-KO-vehicle phenotypes were reproduced in another cohort aimed at testing retro-orbital
241 administration of PHP.eB- Δ N-DGKk (**Sup Fig. 6A-F**). But unlike the mice which received
242 AAVRh10- Δ N-DGKk, (and except for distance travelled during retention phase of NOR, **Sup**
243 **Fig. 6D**), *Fmr1*-KO-PHP.eB- Δ N-DGKk mice showed no significant improvement compared
244 to *Fmr1*-KO-vehicle, suggesting that the level of Δ N-DGKk, although well distributed
245 throughout the brain, was too low to achieve a sufficient effect.
246 Macroorchidism, a well-established phenotype of *Fmr1*-KO model, was not found corrected
247 by the treatments (**Sup Fig. 7**), possibly reflecting a non-neuronal origin.

248

249 **DISCUSSION**

250 FXS is currently uncured as no disease-modifying treatment could be validated despite
251 several clinical trials with investigational drugs (Yamasue et al., 2019). Our data provide
252 evidence that neuron targeted expression of DGKk enzyme with an AAV-based gene therapy
253 approach is able to provide long-term correction of the main behavioral deficits in the young
254 adult *Fmr1*-KO mouse model of FXS (**Sup table 2**).

255 DGKk is an enzyme whose mRNA was previously found to be the main target of FMRP in
256 cortical neurons (Tabet et al., 2016a). We show that DGKk expression is strongly dependent
257 on FMRP and severely altered in FXS brain. In fact, no other protein has been demonstrated
258 to be so critically dependent upon FMRP. Loss of DGKk activity could play a critical role in
259 manifestation of FXS phenotypes because it is a master regulator of second messenger lipids
260 DAG/PA balance and has the potential to be the triggering cause of the many altered neuronal
261 signaling pathways observed in FXS (Tabet et al., 2016b). Removal of the N-terminal part of
262 DGKk does not impact DGKk activity in vitro (Imai et al., 2005), while it abolishes
263 regulation by FMRP. The FMRP-independent Δ N-DGKk protein conserved its ability to
264 modulate cell signaling and showed capacity to rescue a fully developed *Fmr1*-KO mouse
265 brain. At the dose used, intravenous administration of AAVPHP.eB- Δ N-DGKk was unable to
266 rescue the *Fmr1*-KO phenotype, presumably because of insufficient, albeit homogenous
267 expression in the brain. In contrast, intracerebral injection of AAVRh10- Δ N-DGKk led to
268 higher expression of Δ N-DGKk in the mouse brain and correction of disease phenotypes,
269 without affecting survival and with no signs of toxicity several weeks after dosing.

270 Consistently, high Δ N-DGKk expression in neuronal cultures was not associated with cellular

271 toxicity. Rescuing *Fmr1*-KO mouse with AAV-based FMRP administration at an early stage
272 (P0-P5) has provided the first proof of concept of a gene therapy approach for FXS
273 (Gholizadeh et al., 2014; Hampson et al., 2019), but also revealed that inappropriate levels of
274 FMRP expression can lead to worsening of FXS phenotypes, possibly due to the fact that
275 FMRP, like most RNA binding proteins, induces cellular stress when overexpressed (Mazroui
276 et al., 2002). Overall, rescue of *Fmr1*-KO phenotypes with Δ N-DGK κ expression in neurons
277 strengthened the notion that DAG/PA imbalance in neurons is a critical factor of the disease
278 and acting on this imbalance is beneficial for FXS-like condition, including at a late stage of
279 development. Use of Δ N-DGK κ could offer potential for FXS gene therapy, representing a
280 very specific target in the complex pathomechanism of the disease.

281

282 MATERIAL AND METHODS

283

284 **Ethics statement.** Animal work involved in this study was conducted according to ARRIVE
285 guidelines and received authorization from relevant national (Comité National de Réflexion
286 Ethique en Expérimentation Animale).

287

288 **Cloning of human and mouse DGK κ mRNA.** Mouse DGK κ was subcloned from clone
289 IMAGE IRAVp968H03163D. The missing 3' UTR and 5' UTR-N-ter region were cloned by
290 PCR from mouse genomic DNA with primer sets
291 (GCAGCTAGCTCCTTGAAAGCTGGAAGGAGA and AATAGAATGCGGCC-
292 GCCAGCTTCAACAGCACTTGTAG) and
293 (CCAgctgacTTAGACCTCAGAGCTGCGCTAGC and
294 CCAgctagcCCAGGACTCTGGGGCCCTCTCCAT), respectively. The 3' UTR region was
295 introduced at XbaI and NotI sites of the pYX- Δ N DGK κ vector to give pYX- Δ N-DGK κ -
296 3'UTR, and the 5'-UTR-Nter region at Sall-NheI sites of the pYX-DGK κ -3'UTR, NheI site
297 was subsequently deleted by PCR mutagenesis. pCI-mDGK κ -HA and pCI-HA- Δ N-DGK κ
298 were obtained by PCR subcloning into pCI vector (GenBank U47119) with addition of the
299 HA sequence before the STOP codon or after ATG, respectively. Human hDGK κ was
300 subcloned from plasmid pAcGFPC1humDGK κ (Imai et al., 2005) into NheI of pCI vector
301 with addition of 5' and 3'UTRs by PCR cloning to produce pCI-hDGK κ .

302

303 **AAV Δ N-DGK κ vectors construction and preparation.** Δ N-DGK κ HA-tagged DGK κ was
304 cloned under the control of the hSynapsin promoter replacing EGFP in the control plasmid

305 pENN.AAV.hSynapsin.EGFP.RBG (provided by the Penn Vector Core at University of
306 Pennsylvania, Philadelphia) to give pAAV- Δ N-DGK κ . Recombinant adeno-associated virus
307 serotype 9 (AAV9), Rh10 (AAVRh10), PHP.eB (AAVPHP.eB) production was carried out
308 by using the AAV Helper-Free system (Agilent Technologies) with some modifications. AAV
309 vectors were generated by triple transfection of 293T/17 cell line using Polyethylenimine
310 (PEI) and plasmids pAAV-hsynapsin-HA- Δ N-DGK κ or pENN.AAV.hSynapsin.EGFP.RBG
311 together with pHelper (Agilent) and pAAV2/9 or pAAV2/Rh10 (provided by J.Wilson and
312 J.Johnston at Penn Vector Core), or pUCmini-iCAP-PHP.eB (provided by V.Gradinaru and
313 J.Johnston) for serotypes 9, Rh10 and PHP.eB, respectively. Two days after transfection, cells
314 were collected, lysed by three freeze/thaw cycles in dry ice-ethanol and 37 °C baths, further
315 treated with 100 U/mL Benzonase (Novagen) for 30 min at 37 °C, and clarified by
316 centrifugation at 3,000 x g for 15min. Viral vectors were purified by iodixanol (Optiprep,
317 Axis Shield) gradient ultracentrifugation followed by dialysis and concentration against PBS
318 containing 0.5 mM MgCl₂ using centrifugal filters (Amicon Ultra-15.100 K) and filtered
319 through 0.22 μ m (Zolotukhin et al., 2002). Viral particles were quantified by real-time PCR Q-
320 PCR using LightCycler480 SYBR Green I Master (Roche) and primers targeting the flanking
321 sequence of ITR2 (GTAGATAAGTAGCATGGC and CTCCATCACTAGGGGTTTCCTTG)
322 or the flanking sequence of rabbit β -globin polyadenylation signal
323 (CCCTTGAGCATCTGACTTCTGG and AGGGTAATGGGTATTATGGGTGGT). To
324 achieve comparable working concentrations, viruses were diluted to a final concentration of
325 1×10^{13} viral genome per ml (VG/ml) and stored at -80°C until use.

326
327 **Cell culture and transfections.** COS-1 cells were grown in DMEM supplemented with 10%
328 (v/v) FCS and 1 g/L glucose in the presence of antibiotics at 37 °C in 5% CO₂. The day
329 before transfection, 4×10^4 cells were plated into 24-well format plates in 500 μ L of antibiotic-
330 free medium. Transfections of plasmids were performed in triplicate with Lipofectamine 2000
331 (Invitrogen) as directed by the manufacturer with 10 pmol of siRNA (Control or On Target
332 plus Smart Pool mouse *FMRI*; Thermo Fisher Scientific) in a final volume of 600 μ L.
333 Twenty-four hours later, 300 ng of the reporter pCI-DGK κ -HA or pCI-HA- Δ N-DGK κ and 10
334 nM shRNA were cotransfected as above. Twenty-four hours later, cells washed twice in PBS
335 were lysed directly in the loading buffer [100 mM Tris·HCl, pH 6.8, 4% (w/v) SDS, 30%
336 (v/v) glycerol, 1.4M β -mercaptoethanol, and bromophenol blue] for 3 min at 95 °C.

337

338 **Primary cortical neuron cultures and treatments.** Neuron cultures were performed as
339 described in (Tabet et al. 2016). Briefly, cortices from C57BL/6J *Fmr1*^{+/y} or *Fmr1*^{-/y} mouse
340 embryos (embryonic day E17.5) were dissected in 1xPBS, 2.56 mg/mL D-glucose, 3 mg/mL
341 BSA, and 1.16 mM MgSO₄, incubated for 20 min with 0.25 mg/mL trypsin and 0.08 mg/mL
342 DNase I, and mechanically dissociated after supplementation of medium with 0.5 mg/mL
343 trypsin soybean inhibitor, 0.08 mg of DNase I and 1.5 mM MgSO₄. The cells were plated on
344 poly-L-lysine hydrobromide-coated six-well culture plates for 8 days in Neurobasal Medium
345 (GIBCO) supplemented with B27, penicillin/streptomycin, and 0.5 μM L-glutamine. Where
346 indicated, cultures were treated with addition of puromycin solution at the indicated
347 concentrations and times. DGK inhibitors R59022 (DGK Inhibitor I; Calbiochem) and
348 R59949 (DGK Inhibitor II; Calbiochem) were applied at concentrations of 3 and 0.2 μM each
349 for 15 min at 37 °C. After treatment, cells were immediately washed with ice-cold PBS and
350 lysed in 4X Laemmli buffer.

351
352 **Western blot analyses.** Immunoblotting was performed as described previously (Tabet et al.,
353 2016a). Proteins (equivalent to 15 μg) were denatured 5 min at 95°C and resolved by 10%
354 SDS-PAGE. Separated proteins were transferred onto PVDF Immobilon P membrane
355 (Millipore) using a Mini Trans-Blot (Biorad) cell. Membranes were blocked for 1h with TBS-
356 T 1X (Tris-Buffer Saline, pH 7.4 and 0.1% Tween-20 v/v) containing 5% (w/v) BSA or 5%
357 nonfat dry milk. Membranes were incubated overnight at 4°C with primary antibodies diluted
358 in TBS-T buffer containing 5% w/v BSA or milk as follows: mouse anti-FMRP (1C3,
359 1:10,000, IGBMC), purified mouse anti-HA.11 16B12 (1:5000, Biolegend), rabbit anti-
360 hDGKk (1:1000, PA5-25046, ThermoFisher), anti-p-EIF4e Ser209 (1:1000, #9741 Cell
361 Signaling), anti-EIF4 (1:1000 BSA, #9742, Cell Signaling), anti-puromycin (12D10, 1:2000,
362 Sigma-Aldrich), anti-S6 (5G10, 1:1000 #2217S, Cell Signaling), anti-p-S6 (Ser235/236,
363 1:1000, 2211S Cell Signaling), anti-GAPDH (MAB374, 1:10.000, Merck) was used as an
364 internal standard. Membranes were washed in TBS-T buffer and then incubated for an hour at
365 room temperature with the corresponding horseradish peroxidase-conjugated pre-adsorbed
366 secondary antibody (1:5000, blocking solution corresponding, Molecular Probes). Membranes
367 were washed in TBS-T buffer and immunoreactive bands were visualized with the
368 SuperSignal West Pico Chemiluminescent Substrate (Pierce). Immunoblot pictures were
369 acquired using LAS600 GE Amersham and density of the resulting bands was quantified
370 using ImageJ and statistical significance assessed using repeated measures analysis of
371 variance (ANOVA) with Fisher's post hoc comparisons.

372

373 **Analysis of cortical neuron cultures by immunofluorescence microscopy.** Primary cortical
374 neurons grown on poly-L-lysine hydrobromide coated glass coverslips were fixed in 4% (w/v)
375 paraformaldehyde (PFA) in 1xPBS at room temperature (RT) for 20 min, permeabilized with
376 1X PBS and 0.2% Triton X-100 for 10 min at RT, and blocked for 1 h in 1x PBS and 0.1%
377 Triton X-100 with 5% (w/v) BSA. Neurons were incubated with primary antibodies rabbit
378 anti-MAP2 AB5622 (1:500, Merck Millipore), mouse anti-HA.11 16B12 (1:500, Biolegend),
379 mouse anti-NeuN (1:500, MAB377 Merck), rabbit anti-GFAP (1:500, 173002, Synaptic
380 system), overnight at 4 °C. After three washes in 1X PBS and 0.1% Triton X-100 for 10 min,
381 neurons were incubated with secondary goat antibody anti-rabbit (Alexa Fluor 594, 1:1.000,
382 Invitrogen) and anti-mouse (Alexa Fluor 488, 1:1000, Invitrogen), for 1h at RT, and
383 subsequently washed three times in 1xPBS and 0.1% Triton X-100 for 10 min. Coverslips
384 were mounted with antifading medium (Vectashield, Vector) with DAPI and analyzed by
385 fluorescence microscopy. Images were acquired with CellInsight CX7 (Thermo Scientific)
386 using a 10x objective and analyzed with HCS Studio Cell Analysis Software (nuclear
387 segmentation, NeuN and GFAP intensities). Quantification of positive cells for each of
388 these staining was done by applying a threshold manually, based on nuclear segmentation
389 and across 81 fields. Percentage of cells positive for NeuN and GFAP staining was
390 quantified for each well.

391

392 **Caspase 3/7 activity detection.** Caspase 3/7 positives cells were determined with CellEvent
393 Caspase-3/7 Green Detection Reagent following manufacturer instructions. Briefly, primary
394 neurons were prepared as for LDH assays, treated with reagent diluted at 8 μ M in 5% FBS
395 NBM. Positive control wells were treated with apoptotic inducer staurosporine at 0.1 and
396 1 μ M for 6 hours. Cells were fixed with were fixed in 4% (w/v) PFA and nuclei were
397 counterstained with DAPI. Images were acquired with CellInsight CX7 (Thermo Scientific)
398 using a 10x objective and analyzed with HCS Studio Cell Analysis Software (nuclear
399 segmentation and casp3/7 intensities). Quantification of percentage of caspase-3/7 positive
400 cells was done for each well by applying a threshold manually, based on nuclear
401 segmentation and across 81 fields.

402

403 **Lactate dehydrogenase releasing assay.** Lactate dehydrogenase (LDH) release was
404 determined with the Cytotoxicity Detection KitPLUS kit (Roche) following manufacturer
405 instructions. Briefly, primary neurons from Fmr1^{+/-} or Fmr1^{-/-} E17.5 embryos plated at

406 300,000 cells/well in 24-well plate and transduced at 7 DIV with indicated AAV were tested
407 after 7 days. LDH release was measured in microplate reader at 490 nm after 2 hours at 37°C
408 with reaction medium. Maximum LDH release was measured in same conditions after 30min
409 at RT with stop solution. The % of cell death was determined using the formula: % cell death
410 = experimental LDH release /maximum LDH release.

411
412 **Animal housing.** At weaning age (4 weeks), animals were grouped by 3 or 4 individuals from
413 same age and genotype in individually ventilated cages (GM500, Tecniplast, UK), with
414 poplar shaving bedding (Lignocell Select, JRS, Germany), and maintained under standard
415 conditions, on a 12-h light/dark cycle (7h/19h), with standard diet food (standard diet D04,
416 Scientific Animal Food and Engineering, France) and water available ad libitum. Mice from a
417 same cage received the same treatment and were transferred in the animal facility of the
418 phenotyping area the next week.

419
420 **Stereotaxic Surgery and AAV Injections.** Five-week old mice *C57BL/6J Fmr1*^{-/y} or
421 *C57BL/6J Fmr1*^{+y} littermates were deeply anesthetized with ketamine/xylazine
422 (Virbac/Bayer, 100/10 mg/kg, 13 mL/kg, intraperitoneal) dissolved in sterile isotonic saline
423 (NaCl 0.9%) and mounted onto a stereotaxic frame (World Precision Instruments).
424 AAVRh10-DGKκ were injected bilaterally into the striatum (coordinates relative to bregma:
425 anterior-posterior + 0.5 mm; lateral = ±2.2 mm; vertical -3.5 mm) and hippocampus
426 (coordinates relative to bregma: anterior-posterior - 1.7 mm; lateral = ±1.5 mm; vertical -2.0
427 mm) according to the mouse brain atlas (Paxinos G, Franklin KBJ (2001)). A volume of 2.5
428 μL of AAV vector (corresponding to 10¹¹ Genome copies) or saline solution was delivered
429 bilaterally per site of injection with a slow injection rate (0.2 μL/min) through a 32-gauge
430 small hub removable needle mounted on a 10 μL Hamilton syringe connected to a micropump
431 (World Precision Instruments). After each injection was completed, the injector was left in
432 place for an additional 2 min to ensure optimal diffusion and minimize backflow while
433 withdrawing the injector.

434
435 **Retroorbital AAV Injections.** Five-week old mice *C57BL/6J Fmr1*^{-/y} or *C57BL/6J*
436 *Fmr1*^{+y} littermates were deeply anesthetized with ketamine/xylazine (Virbac/Bayer, 100/10
437 mg/kg, 10 mL/kg, intraperitoneal) dissolved in sterile isotonic saline (NaCl 0.9%).
438 AAVPHP.eB-DGKκ were injected retroorbitally with a volume of 80 μL.

439

440 **Analysis of ΔN -DGKk expression in brain sections.** Freshly dissected brains were fixed
441 overnight in PFA 4% and stored in PBS1X prior being processed following Neuroscience
442 Associates procedure <https://www.neuroscienceassociates.com/technologies/multibrain/>.
443 Half-brains were washed in PBS1X solution and embedded in gelatin matrix.
444 MultiBrain[®] cryosections were prepared with 30 μ thickness for free-floating immunolabeling
445 with anti-HA (3F10, 1:150, Sigma) and counter stained with hematoxylin/eosin. Adjacent
446 sections were immunolabelled with anti-NeuN (1:150, MAB377 Merck).

447
448 **Behavioral Experiments.** Behavioral experiments were conducted 4 weeks or 8 weeks after
449 AAV injections to allow sufficient time for viral transduction and DGKk expression.
450 Effective gene expression was assessed by q-PCR to measure viral titer, by western blot and
451 by immuno-histochemistry in 3 different brain areas (cortex, hippocampus and rest of brain).
452 Phenotyping pipeline is described in table 1.

453
454 **Circadian Activity.** Spontaneous locomotor activity and rears are measured using individual
455 cages (20 x 10 x 8 cm) equipped with infra-red captors. The quantity of water and food
456 consumed is measured during the test period using automated pellet feeder and lickometer
457 (Imetronic, Pessac, France). Mice are tested for 32 hours in order to measure habituation to
458 the apparatus as well as nocturnal and diurnal activities. Results are expressed per 1 h periods
459 and/or as a total of the different activities.

460
461 **Elevated plus maze.** The apparatus used is completely automated and made of PVC
462 (Imetronic, Pessac, France). It consists of two open arms (30 X 5 cm) opposite one to the
463 other and crossed by two enclosed arms (30 x 5 x 15 cm). The apparatus is equipped with
464 infrared captors allowing the detection of the mouse in the enclosed arms and different areas
465 of the open arms. Mice were tested for 5 min during which the number of entries into and
466 time spent in the open arms were measured and used as an index of anxiety. Closed arm
467 entries and total arm entries were used as measures of general motor activity.

468
469 **Novel object recognition task.** Mice were tested in a circular arena (50cm diameter and 30cm
470 height basin). The locomotor activity was recorded with the EthoVision XT video tracking
471 system (Noldus, Wageningen, Netherlands). The arena was virtually divided into central and
472 peripheral regions and homogeneously illuminated at 40 Lux. Animals were first habituated to
473 the arena for 15 min. Each mouse was placed in the periphery of the arena and allowed to

474 explore freely the apparatus, with the experimenter out of the animal's sight. The distance
475 traveled and time spent in the central and peripheral regions were recorded over the test
476 session. The percentage of time spent in center area was used as index of emotionality/anxiety.
477 The next day, mice were tested for object recognition in the same arena. They were submitted
478 to a 10-minutes acquisition trial during which they were placed in the arena in presence of a
479 sample objects (A and A') (2.5 cm diameter marble or 2 cm edge plastic dice). The time the
480 animal took to explore the samples (sniffing) was manually recorded. A 10-minutes retention
481 trial was performed 24 h later. During this trial, one of the samples A and another object B
482 (marble or dice depending on acquisition) were placed in the open-field, and the times t_A and
483 t_B the animal took to explore the two objects were recorded. A recognition index (RI) was
484 defined as $(t_B / (t_A + t_B)) \times 100$.

485
486 **Nest building.** On the day of test, mice were singly transferred in a standard cage for the
487 duration of nest building measurement. A block of nesting material (5x5cm hemp square,
488 Happi Mats, Utopia) was placed in the cage. Pictures were taken and visual scoring occurred
489 at 2, 5, 24 h without disturbing the animals. The room temperature was noted when the nest
490 was scored, since nest building has a thermoregulatory function and therefore may be
491 influenced by ambient temperatures. We used a 0-5 scale described by (Gaskill et al., 2013) :
492 0 = undisturbed nesting material; 1 = disturbed nesting material but no nest site; 2 = a flat nest
493 without walls; 3 = a cup nest with a wall less than $\frac{1}{2}$ the height of a dome that would cover a
494 mouse; 4 = an incomplete dome with a wall $\frac{1}{2}$ the height of a dome; 5 = a complete dome
495 with walls taller than $\frac{1}{2}$ the height of a dome, which may or may not fully enclose the nest.

496
497 **Social recognition test.** Social recognition test evaluates the preference of a mouse for a
498 congener as compared to an object placed in an opposite compartment. This test is also used
499 for evaluation of social memory by measuring exploration of a novel congener as compared to
500 a familiar one. Social behavior is altered in several diseases such as autism and mental
501 retardation. The apparatus is a transparent cage composed with a central starting compartment
502 and 2 side compartments where circular grid cup (goal box) is placed at each extremity, and
503 where the congener can be placed during testing. Testing was performed for 2 consecutive
504 days. On the first day, the mouse was placed in central box then allowed to explore freely the
505 apparatus for 10 min in order to attenuate their emotionality. On the second day, a C57Bl/6
506 congener from the same sex was placed in one goal box and an object was placed in the
507 opposite one. The mouse was then placed in the starting central compartment and allowed to

508 explore freely the apparatus for 10 min. The position of the congener and object boxes was
509 counterbalanced to avoid any potential spatial preference. The duration of exploration of each
510 goal box (when the mouse is sniffing the grid delimiting the goal box) was manually
511 measured and the percentage of time the mouse took to explore the congener was used as
512 index of social preference (recognition preference). A 10min retention trial was then
513 performed during which the object was replaced by a novel congener. The duration of
514 exploration of each goal box was manually measured and the percentage of time the mouse
515 takes to explore the congener was used as index of social memory. The social preference
516 index (SR) is defined as $(\text{time Congener} / (\text{time Object} + \text{time Congener})) \times 100$; and the
517 social memory index as $(\text{time novel Congener} / (\text{familiar congener} + \text{time novel Congener}))$
518 $\times 100$.

519
520 **Lipidomic analyzes.** Nitrogen frozen brain samples (cortex, hippocampus, rest) were let thaw
521 on ice and mechanically homogenized with 1 vol H₂O with Precellys 24 system during
522 2x15sec at 4°C and 5300 rpm. Protein concentration of sample was adjusted at 5 mg/ml
523 concentration and lipids were analyzed on Lipotype GmbH platform. Lipids were extracted
524 using chloroform and methanol (Sampaio et al., 2011) with Hamilton Robotics STARlet.
525 Samples were spiked with lipid class-specific internal standards prior to extraction. After
526 drying and resuspending in MS acquisition mixture, lipid extracts were subjected to mass
527 spectrometric analysis. Mass spectra were acquired on a hybrid quadrupole/Orbitrap mass
528 spectrometer (Thermo Scientific Q-Exactive) equipped with an automated nano-flow
529 electrospray ion source in both positive and negative ion mode. Lipid identification using
530 LipotypeXplorer (Herzog et al., 2011) was performed on unprocessed (*.raw format) mass
531 spectra. For MS-only mode, lipid identification was based on the molecular masses of the
532 intact molecules. MSMS mode included the collision induced fragmentation of lipid
533 molecules and lipid identification was based on both the intact masses and the masses of the
534 fragments. Prior to normalization and further statistical analysis lipid identifications were
535 filtered according to mass accuracy, occupation threshold, noise and background. Intensity of
536 lipid class-specific internal standards was used for lipid quantification. The identified lipid
537 molecules were quantified by normalization to a lipid class specific internal standard. The
538 amounts in pmol of individual lipid molecules (species of subspecies) of a given lipid class
539 were summed to yield the total amount of the lipid class. The amounts of the lipid classes
540 were normalized to the total lipid amount yielding mol% per total lipids.

541

542 **Statistical analyses.** Quantitative data were analyzed using single or repeated measures
543 analysis of variance (ANOVA) and Student Newman Keuls test. For the comparison with
544 chance, one group t-test was used. Qualitative parameters (nesting) were analyzed using χ^2
545 test. The level of significance was set at $p < 0.05$.

546

547 **References**

548 The Dutch-Belgian Fragile X Consortium. (1994). Fmr1 knockout mice: a model to study
549 fragile X mental retardation. *Cell* 78, 23-33.

550 Bear, M.F., Huber, K.M., and Warren, S.T. (2004). The mGluR theory of fragile X mental
551 retardation. *Trends Neurosci* 27, 370-377.

552 Chan, K.Y., Jang, M.J., Yoo, B.B., Greenbaum, A., Ravi, N., Wu, W.L., Sanchez-Guardado, L.,
553 Lois, C., Mazmanian, S.K., Deverman, B.E., *et al.* (2017). Engineered AAVs for efficient
554 noninvasive gene delivery to the central and peripheral nervous systems. *Nat Neurosci* 20,
555 1172-1179.

556 Dolen, G., Osterweil, E., Rao, B.S., Smith, G.B., Auerbach, B.D., Chattarji, S., and Bear, M.F.
557 (2007). Correction of fragile X syndrome in mice. *Neuron* 56, 955-962.

558 Gantois, I., Khoutorsky, A., Popic, J., Aguilar-Valles, A., Freemantle, E., Cao, R., Sharma, V.,
559 Pooters, T., Nagpal, A., Skalecka, A., *et al.* (2017). Metformin ameliorates core deficits in a
560 mouse model of fragile X syndrome. *Nat Med* 23, 674-677.

561 Gaskill, B.N., Karas, A.Z., Garner, J.P., and Pritchett-Corning, K.R. (2013). Nest building as an
562 indicator of health and welfare in laboratory mice. *J Vis Exp*, 51012.

563 Gholizadeh, S., Arsenault, J., Xuan, I.C., Pacey, L.K., and Hampson, D.R. (2014). Reduced
564 phenotypic severity following adeno-associated virus-mediated Fmr1 gene delivery in fragile
565 X mice. *Neuropsychopharmacology* 39, 3100-3111.

566 Gkogkas, C.G., Khoutorsky, A., Cao, R., Jafarnejad, S.M., Prager-Khoutorsky, M., Giannakas,
567 N., Kaminari, A., Fragkouli, A., Nader, K., Price, T.J., *et al.* (2014). Pharmacogenetic inhibition
568 of eIF4E-dependent Mmp9 mRNA translation reverses fragile X syndrome-like phenotypes.
569 *Cell Rep* 9, 1742-1755.

570 Gross, C., Chang, C.W., Kelly, S.M., Bhattacharya, A., McBride, S.M., Danielson, S.W., Jiang,
571 M.Q., Chan, C.B., Ye, K., Gibson, J.R., *et al.* (2015). Increased expression of the PI3K enhancer
572 PIKE mediates deficits in synaptic plasticity and behavior in fragile X syndrome. *Cell Rep* 11,
573 727-736.

574 Guo, W., Murthy, A.C., Zhang, L., Johnson, E.B., Schaller, E.G., Allan, A.M., and Zhao, X.
575 (2012). Inhibition of GSK3beta improves hippocampus-dependent learning and rescues
576 neurogenesis in a mouse model of fragile X syndrome. *Hum Mol Genet* *21*, 681-691.

577 Hagerman, R.J., Berry-Kravis, E., Hazlett, H.C., Bailey, D.B., Jr., Moine, H., Kooy, R.F., Tassone,
578 F., Gantois, I., Sonenberg, N., Mandel, J.L., *et al.* (2017). Fragile X syndrome. *Nat Rev Dis*
579 *Primers* *3*, 17065.

580 Hampson, D.R., Hooper, A.W.M., and Niibori, Y. (2019). The Application of Adeno-Associated
581 Viral Vector Gene Therapy to the Treatment of Fragile X Syndrome. *Brain Sci* *9*.

582 Herzog, R., Schwudke, D., Schuhmann, K., Sampaio, J.L., Bornstein, S.R., Schroeder, M., and
583 Shevchenko, A. (2011). A novel informatics concept for high-throughput shotgun lipidomics
584 based on the molecular fragmentation query language. *Genome Biol* *12*, R8.

585 Imai, S., Kai, M., Yasuda, S., Kanoh, H., and Sakane, F. (2005). Identification and
586 characterization of a novel human type II diacylglycerol kinase, DGK kappa. *J Biol Chem* *280*,
587 39870-39881.

588 Jiang, Y., Sakane, F., Kanoh, H., and Walsh, J.P. (2000). Selectivity of the diacylglycerol kinase
589 inhibitor 3-[2-(4-[bis-(4-fluorophenyl)methylene]-1-piperidinyl)ethyl]-2, 3-dihydro-2-thioxo-
590 4(1H)quinazolinone (R59949) among diacylglycerol kinase subtypes. *Biochem Pharmacol* *59*,
591 763-772.

592 Kaufmann, W.E., Cortell, R., Kau, A.S., Bukelis, I., Tierney, E., Gray, R.M., Cox, C., Capone,
593 G.T., and Stanard, P. (2004). Autism spectrum disorder in fragile X syndrome:
594 communication, social interaction, and specific behaviors. *Am J Med Genet A* *129A*, 225-234.

595 Mazroui, R., Huot, M.E., Tremblay, S., Filion, C., Labelle, Y., and Khandjian, E.W. (2002).
596 Trapping of messenger RNA by Fragile X Mental Retardation protein into cytoplasmic
597 granules induces translation repression. *Hum Mol Genet* *11*, 3007-3017.

598 Mientjes, E.J., Nieuwenhuizen, I., Kirkpatrick, L., Zu, T., Hoogeveen-Westerveld, M.,
599 Severijnen, L., Rife, M., Willemsen, R., Nelson, D.L., and Oostra, B.A. (2006). The generation
600 of a conditional Fmr1 knock out mouse model to study Fmrp function in vivo. *Neurobiol Dis*
601 *21*, 549-555.

602 Pasciuto, E., Ahmed, T., Wahle, T., Gardoni, F., D'Andrea, L., Pacini, L., Jacquemont, S.,
603 Tassone, F., Balschun, D., Dotti, C.G., *et al.* (2015). Dysregulated ADAM10-Mediated
604 Processing of APP during a Critical Time Window Leads to Synaptic Deficits in Fragile X
605 Syndrome. *Neuron* *87*, 382-398.

606 Qin, M., Kang, J., Burlin, T.V., Jiang, C., and Smith, C.B. (2005). Postadolescent changes in
607 regional cerebral protein synthesis: an in vivo study in the FMR1 null mouse. *J Neurosci* 25,
608 5087-5095.

609 Sampaio, J.L., Gerl, M.J., Klose, C., Ejsing, C.S., Beug, H., Simons, K., and Shevchenko, A.
610 (2011). Membrane lipidome of an epithelial cell line. *Proc Natl Acad Sci U S A* 108, 1903-
611 1907.

612 Sidhu, H., Dansie, L.E., Hickmott, P.W., Ethell, D.W., and Ethell, I.M. (2014). Genetic removal
613 of matrix metalloproteinase 9 rescues the symptoms of fragile X syndrome in a mouse
614 model. *J Neurosci* 34, 9867-9879.

615 Sonenberg, N. (1994). Regulation of translation and cell growth by eIF-4E. *Biochimie* 76, 839-
616 846.

617 Tabet, R., Moutin, E., Becker, J.A., Heintz, D., Fouillen, L., Flatter, E., Krezel, W., Alunni, V.,
618 Koebel, P., Dembele, D., *et al.* (2016a). Fragile X Mental Retardation Protein (FMRP) controls
619 diacylglycerol kinase activity in neurons. *Proc Natl Acad Sci U S A* 113, E3619-3628.

620 Tabet, R., Vitale, N., and Moine, H. (2016b). Fragile X syndrome: Are signaling lipids the
621 missing culprits? *Biochimie*.

622 Wang, X., Flynn, A., Waskiewicz, A.J., Webb, B.L., Vries, R.G., Baines, I.A., Cooper, J.A., and
623 Proud, C.G. (1998). The phosphorylation of eukaryotic initiation factor eIF4E in response to
624 phorbol esters, cell stresses, and cytokines is mediated by distinct MAP kinase pathways. *J*
625 *Biol Chem* 273, 9373-9377.

626 Westmark, C.J., Westmark, P.R., O'Riordan, K.J., Ray, B.C., Hervey, C.M., Salamat, M.S.,
627 Abozeid, S.H., Stein, K.M., Stodola, L.A., Tranfaglia, M., *et al.* (2011). Reversal of fragile X
628 phenotypes by manipulation of AbetaPP/Abeta levels in Fmr1KO mice. *PLoS One* 6, e26549.

629 Yamasue, H., Aran, A., and Berry-Kravis, E. (2019). Emerging pharmacological therapies in
630 fragile X syndrome and autism. *Curr Opin Neurol* 32, 635-640.

631 Zolotukhin, S., Potter, M., Zolotukhin, I., Sakai, Y., Loiler, S., Fraitas, T.J., Jr., Chiodo, V.A.,
632 Phillipsberg, T., Muzyczka, N., Hauswirth, W.W., *et al.* (2002). Production and purification of
633 serotype 1, 2, and 5 recombinant adeno-associated viral vectors. *Methods* 28, 158-167.

634

635

636 **Acknowledgements:**

637 We thank Flora Tassone and Veronica Martinez-Cerdeno for human brain materials. We are
638 indebted to Antonina Fedorova, H el ene Puccio, Yann Herault, Sirine Souali-crespo, Tania
639 Sorg-Guss and members of Lysogene team for discussions and suggestions. We are grateful
640 to Andr ea Geoffroy and members of Institut Clinique de la Souris for help with the behavioral
641 studies, Pascale Koebel for AAV preparations, Eric Flatter for technical assistance, Nadine
642 Banquart-Ott and Chadia Nahy for mice care, Anne Maglott for toxicity analyses, Erwan
643 Grandgirard for help with imaging, IGBMC core facilities, Zaiane Schmitt and Fumi Hoshino
644 for technical assistance. We specially thank Laura Benkemoun and Fondation Maladies Rares
645 for support and suggestions. We are grateful to colleagues of J. Chelly team for discussions.

646

647 **Funding:**

648 This work was supported by Satt Conectus program GETEX, ANR-18-CE12-0002-01 and
649 Fondation J er me Lejeune funding to HM and by Fond Paul Mandel to KH and Fondation
650 pour la Recherche M edicale to BZ. This study was also supported by ANR-10-LABX-0030-
651 INRT under the frame program Investissements d’Avenir ANR-10-IDEX-0002-02.

652 **Competing interests:** HM and RT are listed as inventors on a patent describing the AAV
653 construct reported in this manuscript. M.H., and R.L. are full-time employees and hold equity
654 in Lysogene. All other authors declare no competing interests.

655

656 **Author contributions**

657 K.H., O.C, B.Z., and F.P. designed and performed experiments and helped writing the
658 manuscript. D.D. performed statistical analyses. R.T., M.H., R.L. helped designing the
659 experiments and writing manuscript. H.M. supervised the project, designed experiments and
660 wrote the manuscript.

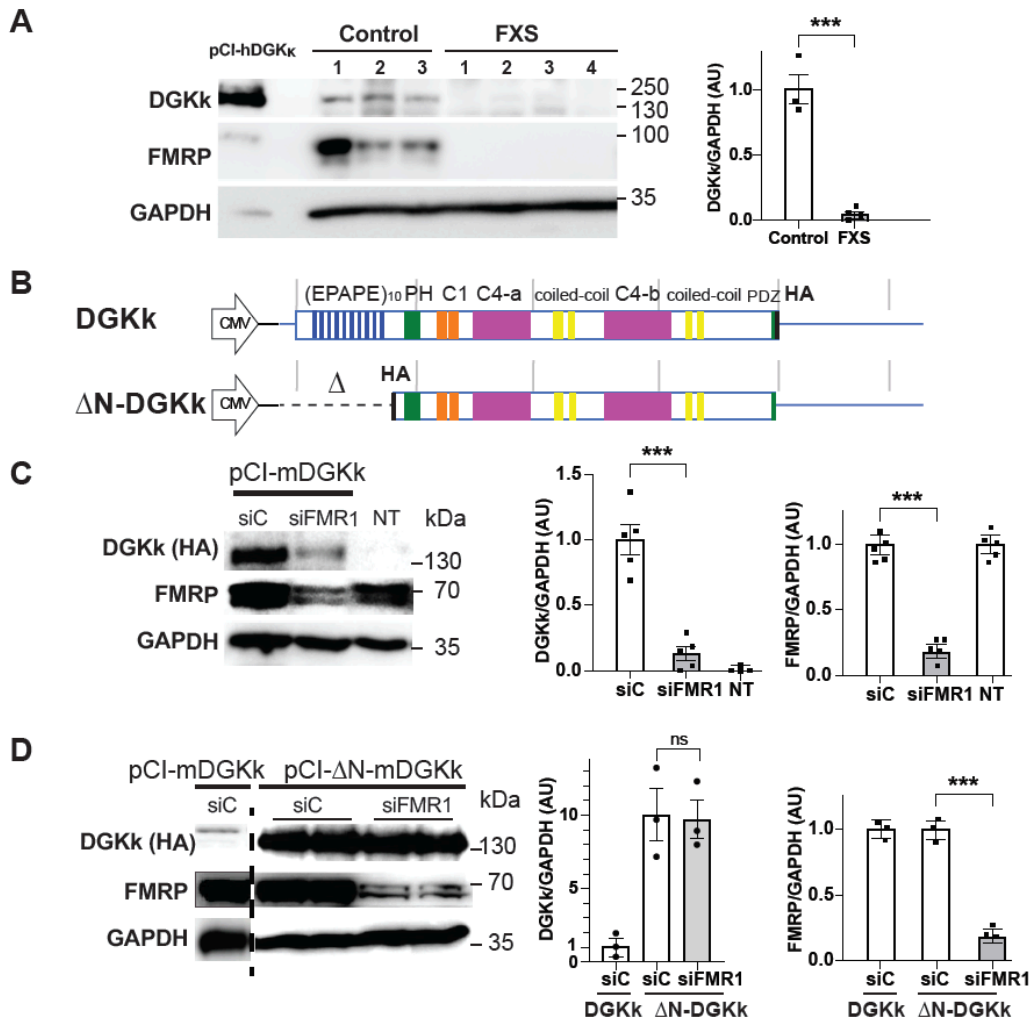
661

662

663 **Figure**

Fig. 1

Habbas et al.



664

665

666

667

668

669

670

671

672

673

674

675

676

677

678

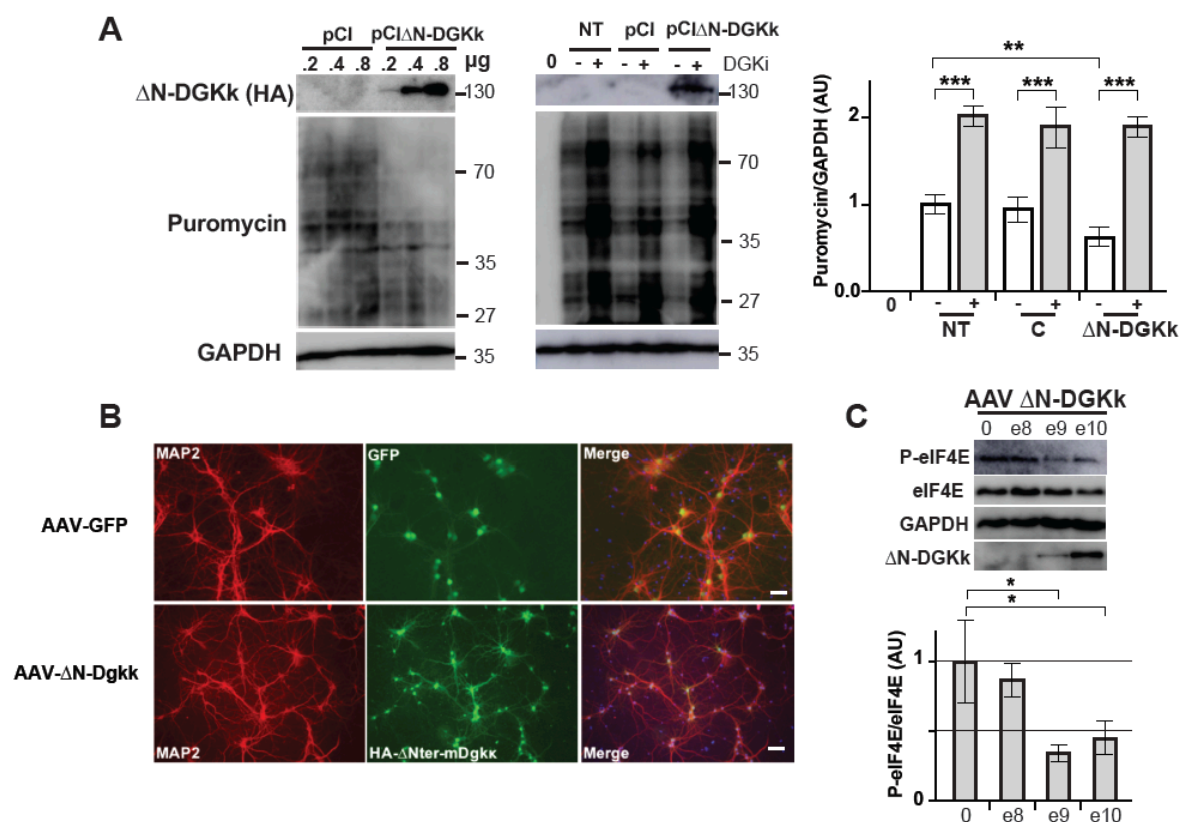
679

680

681

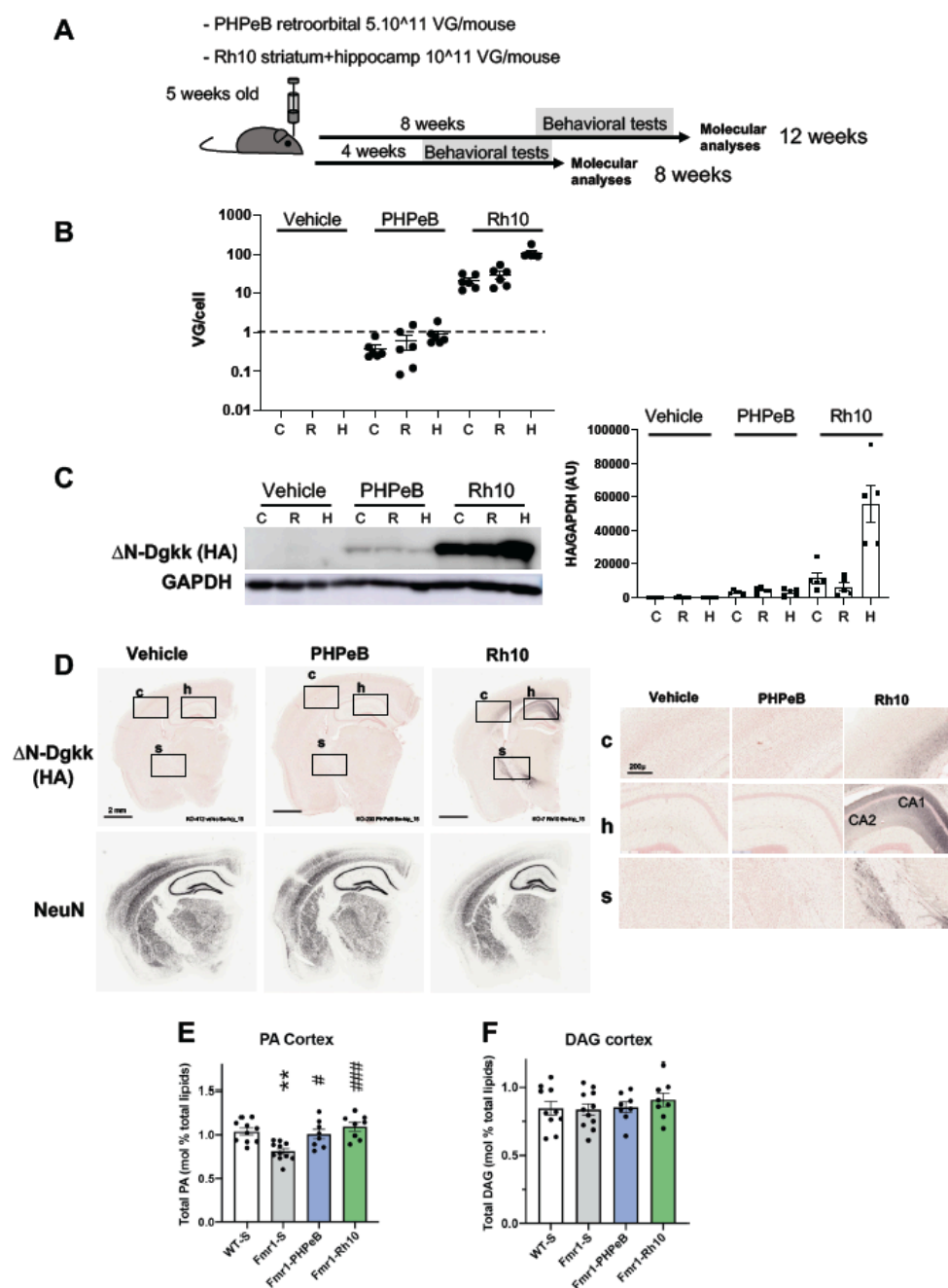
682

Fig. 1 : DGKk expression is altered in FXS and FMRP is required for translation control via its N-terminal domain. **A)** Western blot analysis of lysates from cerebellum of control (n = 3) and FXS patients “FXS” (n = 4). HeLa cell extract transfected with pCI-hDGKκ was used as antibody specificity control and size marker. Representative images of immunoblots probed with antibodies against the indicated proteins are shown. GAPDH was the loading control. Quantification of Western blots is shown on right. Protein amounts of DGKk are normalized to GAPDH and presented as fold change relative to control. **B)** Schematic map of DGKk constructs used for the transfection experiments and subsequent vector preparations. The different domains of the protein are indicated and represented at scale (repeated EPAPE, Pleckstrin Homology PH domain, phorbol ester/diacyl glycerol binding C1 domain, catalytic split C4 a and b domains, putative PDZ binding motive, HA-tag, grey bars interval 1kB), 5' and 3' UTR regions are represented with blue line, 3'UTR not at scale (3.8 kB). **C)** Immunoblots and quantification of lysates from Cos-1 cells transfected with plasmid pCI-mDGKκ-HA or mock transfected (NT) and pre-transfected 24h before with siRNA control (siC) or against FMRP (siFMR1). GAPDH was used as a loading control. For quantification, the DGKk and FMRP signals were normalized against GAPDH signal and presented relative to the signal for siC treated cells (n = 5 in each group). **D)** Immunoblots and quantification of lysates from Cos-1 cells transfected with plasmid pCI-HA-ΔN-DGKκ or pCI-mDGKκ-HA and pre-treated with siRNA control (siC) or against FMRP (siFMR1). Quantifications as in C. Each point represents data from an individual culture, and all values are shown as mean ± SEM ***P < 0.001, **P < 0.01, *P < 0.05 calculated by unpaired Student T test.



683

684 **Fig. 2 : ΔN-DGKk expression impacts cellular signaling.** **A)** Immunoblots and
685 quantification of lysates from Cos-1 cells transfected with plasmid pCI-HA-ΔN-DGKk,
686 untransfected (NT), or plasmid pCI control, with the indicated amount of plasmid (μg) and
687 incubated with puromycin to measure basal rates of protein synthesis. GAPDH was used as a
688 loading control. 0 indicates no puromycin treatment, -/+ indicates treatment without or with
689 DGK inhibitor (DGKi) 3 μM R59022 and 0.2 μM R59949 at 6 μM, 15 min. Densitogram of
690 puromycin incorporation is presented as change relative to mock transfected conditions ($n =$
691 3). **B)** Representative immunofluorescence staining of cortical neuron cultures transduced at 8
692 DIV (days in vitro) with 10e9 VG/ml culture volume AAVRh10 GFP or ΔN-DGKk and
693 assessed after 5 days using anti-MAP2 and anti-HA for ΔN-DGKk or direct 488 nm excitation
694 for GFP, Dapi was used to visualize nuclei on merged images. Scale bar, 40 μm. **C)**
695 Representative immunoblots of lysates from cortical neurons transduced with AAVRh10-ΔN-
696 DGKk (AAV ΔN-DGKk), at the indicated titers (VG/ml culture volume) and quantification of
697 phosphorylation and total levels of eIF4E. GAPDH was used as a loading control. For
698 quantification, the phospho-protein signal was normalized against total protein signal and is
699 presented relative to the signal for vehicle-treated cultures. Each point represents data from an
700 individual culture, and all values are shown as mean ± SEM * $P < 0.05$ calculated by One
701 way-ANOVA with Tukey's multiple comparison test ($n = 3$ individual cultures).

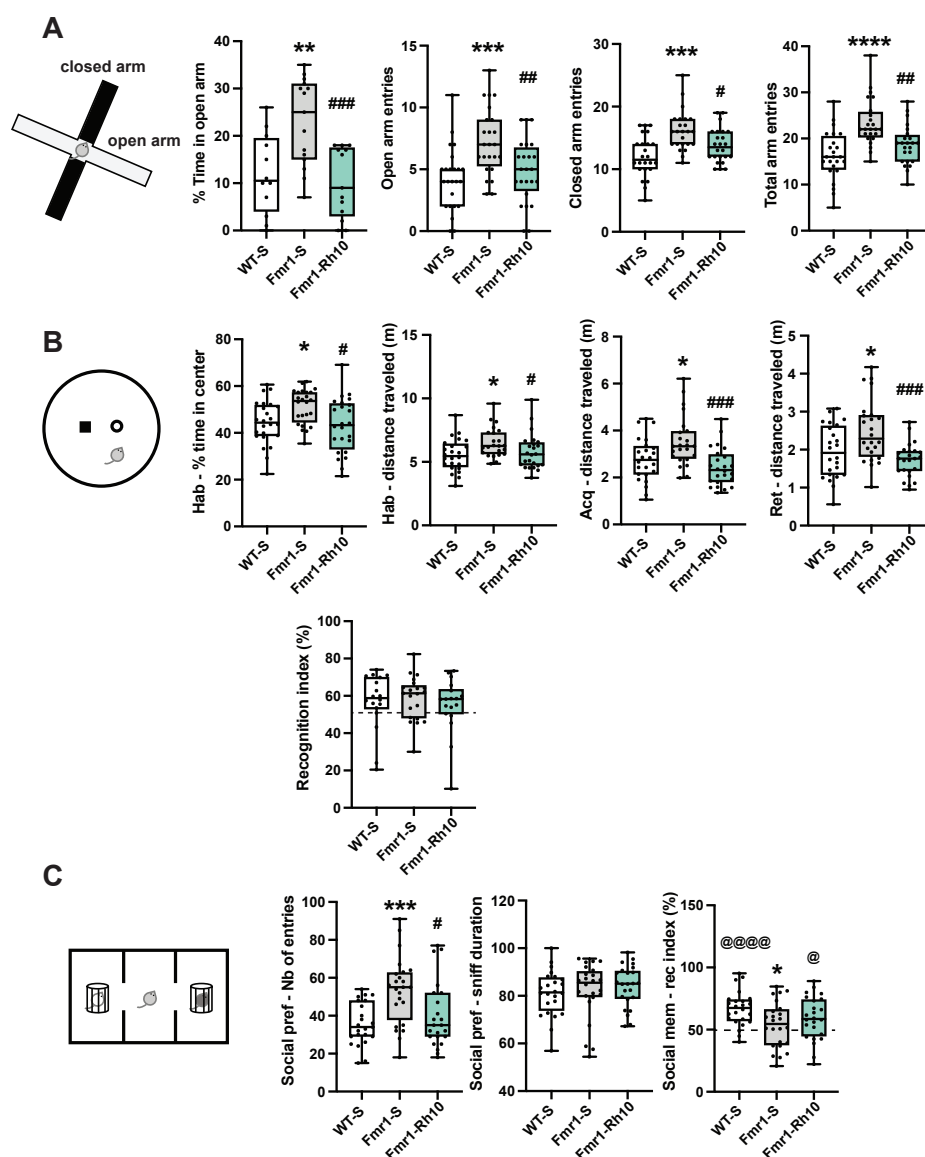


702

703 **Fig. 3 : Δ N-DGKk expression in vivo with AVV vectors corrects abnormal cortical phosphatidic acid level**
 704 **of Fmr1-KO mice.** **A**) Scheme of timeline analyses performed. **B**) Viral titers (viral genome copy VG per cell)
 705 determined by qPCR in cortical, hippocampal and rest of brain areas of Fmr1-KO mice treated with saline
 706 solution (Vehicle), AAVPHP.eB- Δ N-DGKk (PHP.eB), AAVRh10- Δ N-DGKk (Rh10) 8 weeks after injections.
 707 Data are mean \pm SEM. Each dot represents an individual mouse. **C**) Immunoblots and quantification of Δ N-
 708 DGKk protein in lysates from brain areas of mice treated as in B. GAPDH was used as a loading control.
 709 Densitogram of Δ N-DGKk expression is presented as change relative to vehicle conditions. Data are mean \pm
 710 SEM ($n = 5$). **D**) Representative coronal brain sections processed for detection of Δ N-DGKk using
 711 immunohistochemistry on Fmr1-KO mice treated with indicated treatment, 8 weeks post-injections, counter
 712 stained with eosin hematoxylin. Adjacent sections were immunolabelled with NeuN. 3 mice per genotype were
 713 processed. The sections shown are between Bregma levels -1.50 mm and -1.80 mm. Scale bar is 2 mm.
 714 Magnifications of regions of cortex (c), hippocampus (h), and striatum (s) are shown in side panels, scale bar
 715 200 μ m. **E**) Total phosphatidic acid (PA) level measure by mass spectrometry in cortex of WT mice treated with
 716 saline solution (WT-S) and Fmr1-KO mice treated with saline (Fmr1-S), AAVPHP.eB- Δ N-DGKk (Fmr1-
 717 PHP.eB), AAVRh10- Δ N-DGKk (Fmr1-Rh10) 8 weeks after injections. Data are expressed as mean \pm SEM of
 718 mol % of total lipids and analyzed using one-way ANOVA and Tukey's multiple comparisons test, $**p < 0.01$,
 719 $n = 8$ individual animals, except for WT $n = 7$. **F**) Total diacylglycerol (DAG) level in cortex measured as in E).

Fig. 4

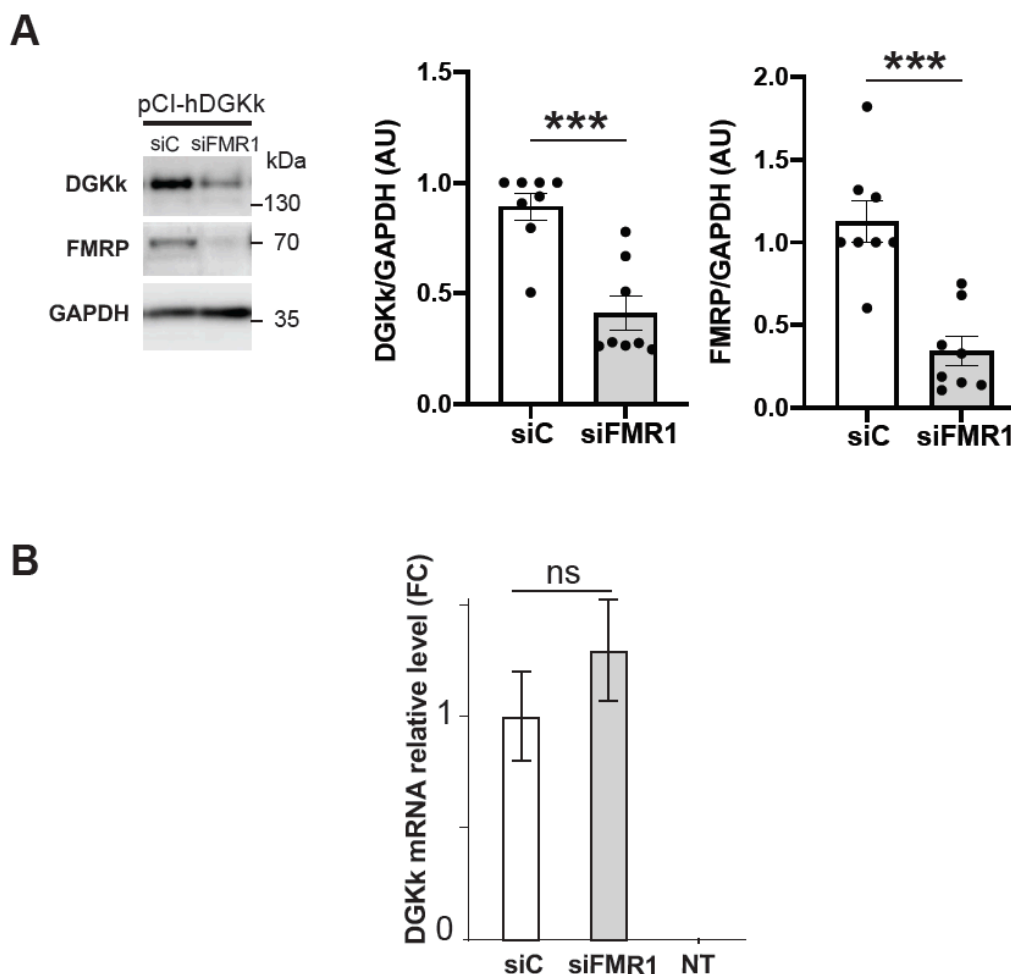
Habbas et al.



720
 721 **Fig. 4 : AAVRh10-ΔN-DGKk rescues behavior alterations of *Fmr1*-KO mouse 4 weeks**
 722 **after injections.** **A)** Elevated Plus Maze. Percentage of time spent in open arms and number
 723 of entries in open, closed and total (open+closed) arms. **B)** Novel object recognition.
 724 Locomotor activity (distance in m) in the whole arena and percentage of time spent in the
 725 center during 15 min habituation. Locomotor activity during the acquisition and retention
 726 trials. Recognition index. **C)** Stereotypies. Number of digging. **D)** Social recognition. Number
 727 of entries in the two side compartments during preference session (left), social preference
 728 (percentage of exploration of a congener vs an object) (center) and social memory (percentage
 729 of exploration of a novel vs familiar congener) (right). Data are expressed as median with
 730 interquartile range with minimum and maximum values and analyzed using one-way
 731 ANOVA and Tukey's multiple comparisons test and one group t-test. * p<0.05, **p<0.01,
 732 ***p<0.001, ****p<0.0001 vs WT-S; # p<0.05, ## p<0.01, ### p<0.001 vs Fmr1-S; @
 733 p<0.05, @@ p<0.01, @@@@ p<0.0001 vs chance (50%).

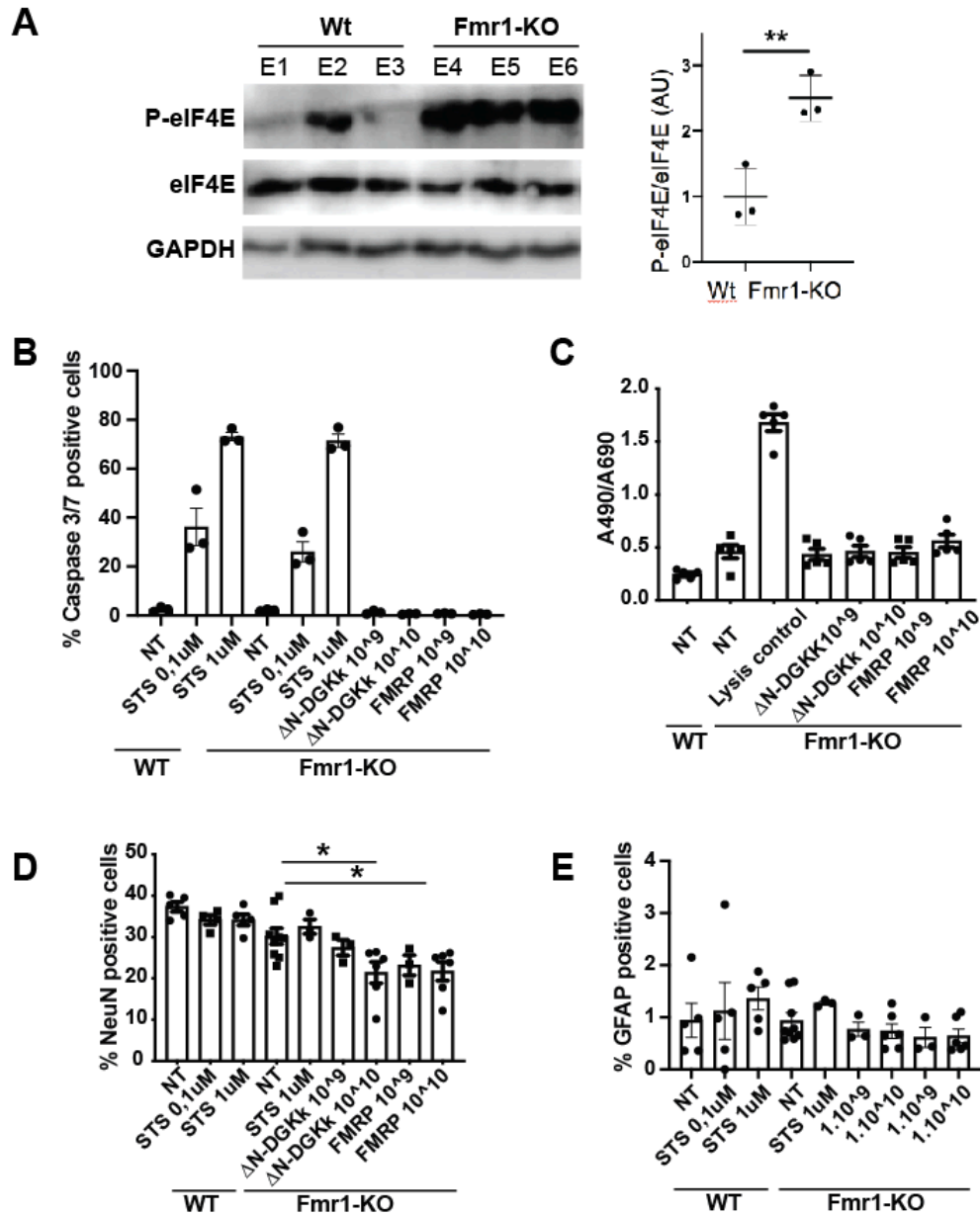
734

735 **Supplementary material**



736

737 **Supplementary Fig. 1 : Influence of FMRP protein on human DGKk protein expression**
738 **and on mouse DGKk mRNA level.** **A)** Immunoblots and quantification of lysates from HeLa
739 cells transfected with plasmid pCI-hDGK κ encoding human DGKk and pre-transfected 24h
740 before with siRNA control (siC) or against FMRP (siFMR1). GAPDH was used as a loading
741 control. For quantification, DGKk and FMRP signals were normalized against GAPDH signal
742 and presented relative to the signal for siC treated cells. Each point represents data from an
743 individual culture, and all values are shown as mean \pm SEM *** $P < 0.001$, calculated by
744 unpaired Student T test. **B)** Quantification of mouse DGK κ mRNA by qRT-PCR in RNA
745 extracts of Cos-1 cells transfected with plasmid pCI-mDGK κ -HA and pre-transfected with
746 siRNA control (siC) or siRNA against FMRP (siFMR1) or mock transfected (NT). Data are
747 means of fold change \pm SEM, determined using $\Delta\Delta C_t$ method with Actb as normalizer, n = 3
748 biological replicates.

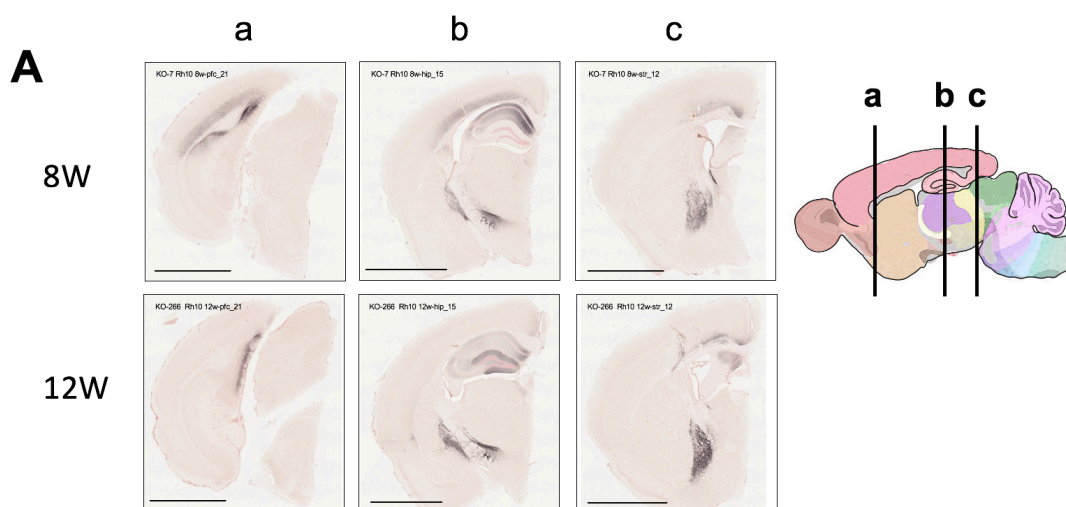


749

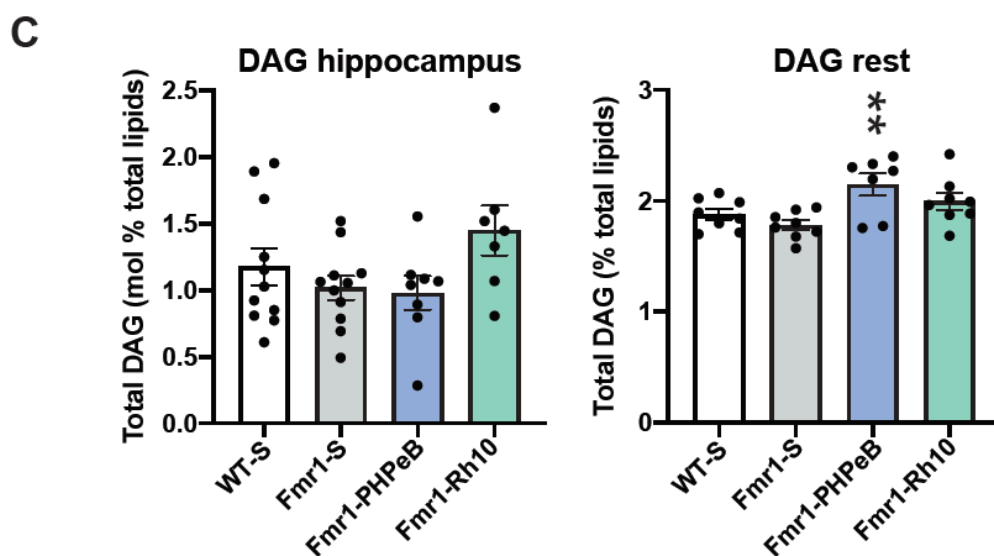
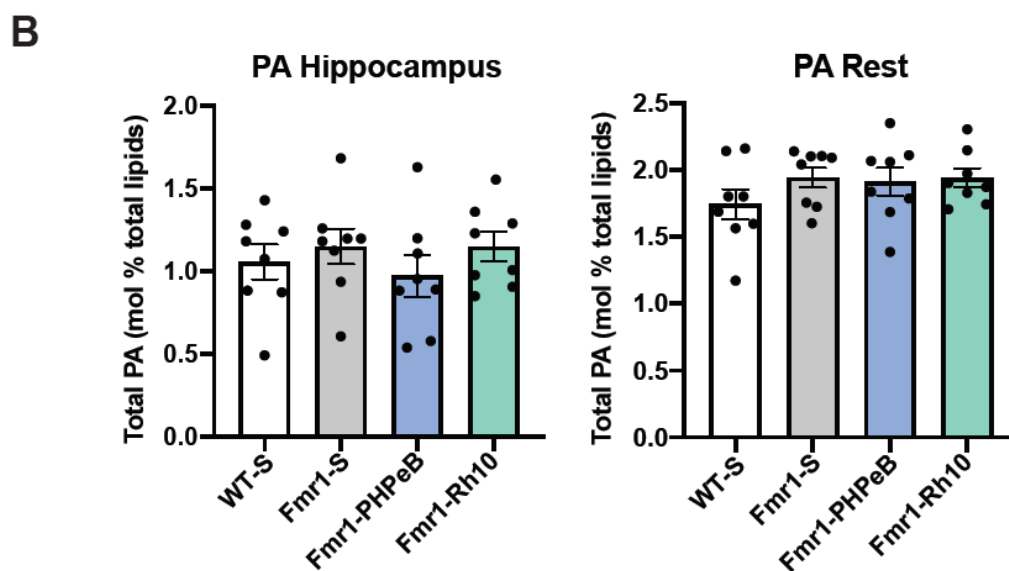
750 **Supplementary Fig. 2 : Phosphorylation of eIF4E is increased in Fmr1-KO cortical**
 751 **neurons compared to WT, and ΔN-DGKk expression in neurons does not lead to**
 752 **toxicity.** **A)** Representative immunoblots of lysates from WT and Fmr1-KO cortical neurons
 753 and quantification of phosphorylation and total levels of eIF4E. GAPDH was used as a
 754 loading control. For quantification, the phospho-protein signal was normalized first against
 755 total protein signal and is presented relative to the signal for WT culture. Each point
 756 represents data from an individual culture, and all values are shown as mean ± SEM ** $P <$
 757 0.01 by Student T test ($n = 3$ individual cultures). Quantification of caspase 3/7 activity (**B**),
 758 release of lactate dehydrogenase (LDH) (**C**), percentage of NeunN (**D**) and GFAP (**E**) positive
 759 cells, in WT and Fmr1-KO cortical neurons untreated (NT) or transduced at 8 DIV for 8 DIV
 760 with indicated titers of AAV (viral genome copies) AAVRh10-ΔN-DGKk or AAVRh10-
 761 FMRP by immunofluorescence high throughput cell imaging. Positive control wells were
 762 treated with apoptotic inducer staurosporine (STS) at 0.1 and 1μM for 6 hours. Data are mean
 763 ± SEM and analyzed using one-way ANOVA and Tukey's multiple comparisons test. *
 764 $p < 0.05$.

Sup Fig. 3

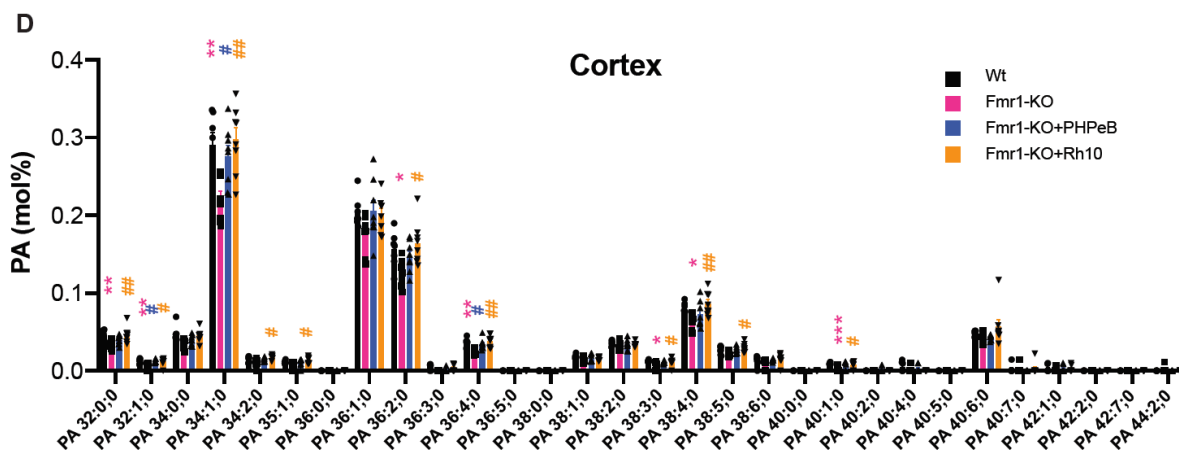
Habbas et al.



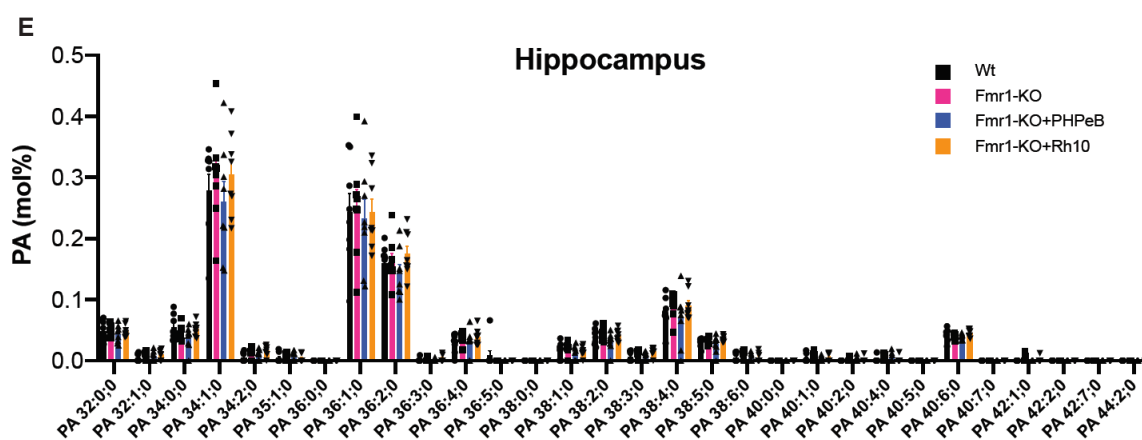
765



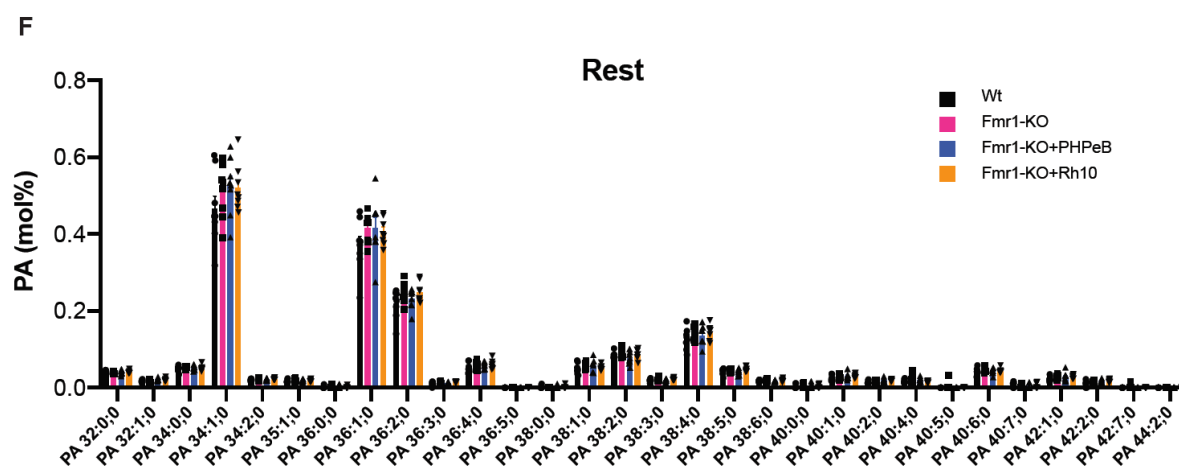
766



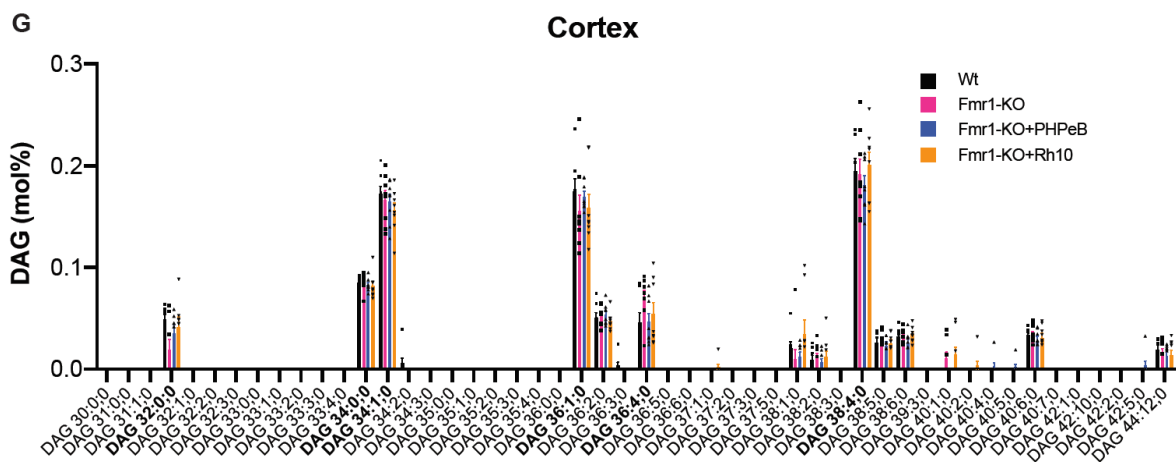
767



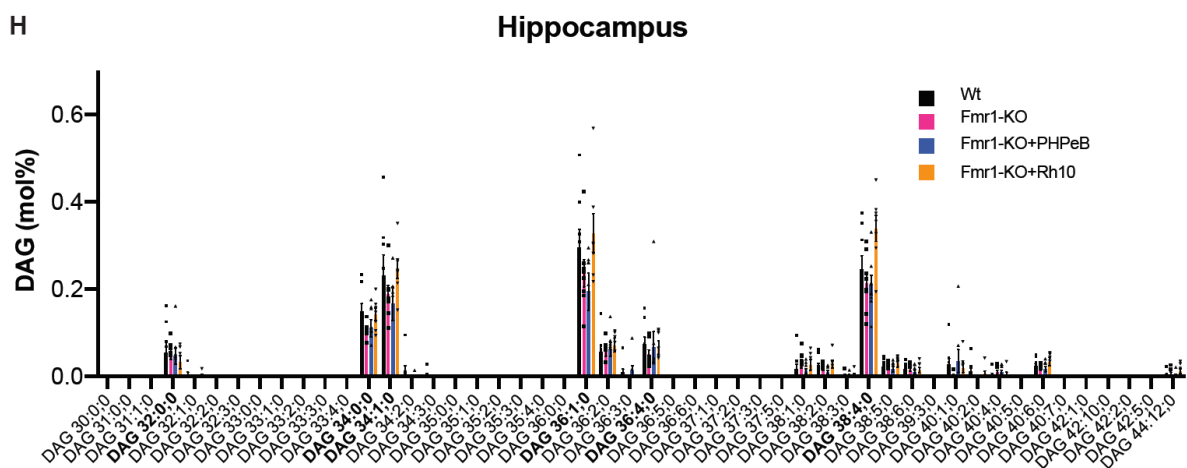
768



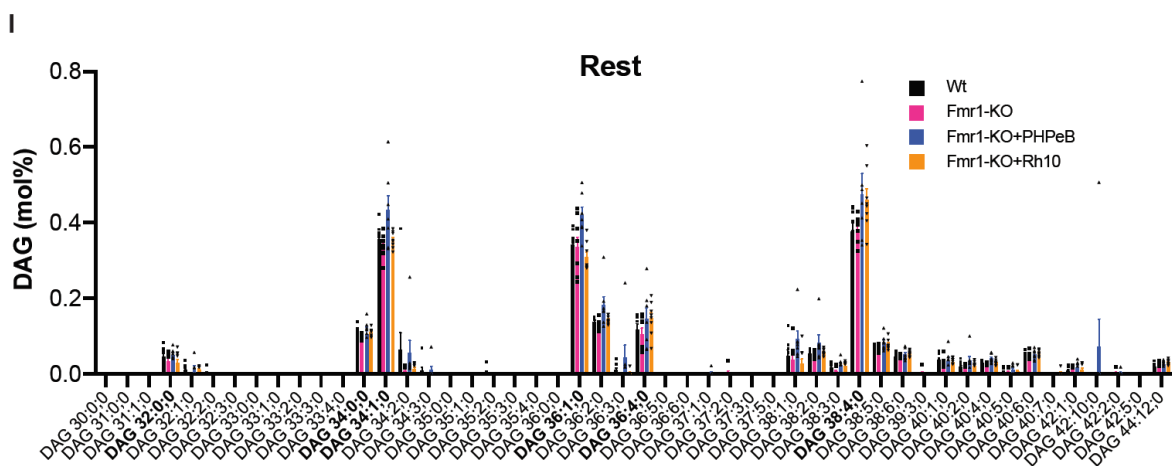
769



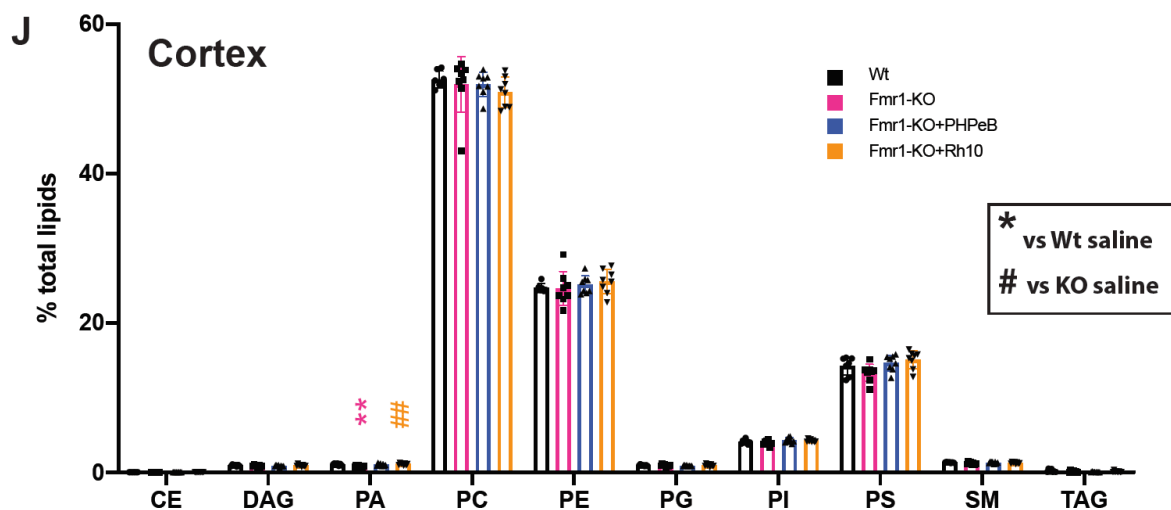
770



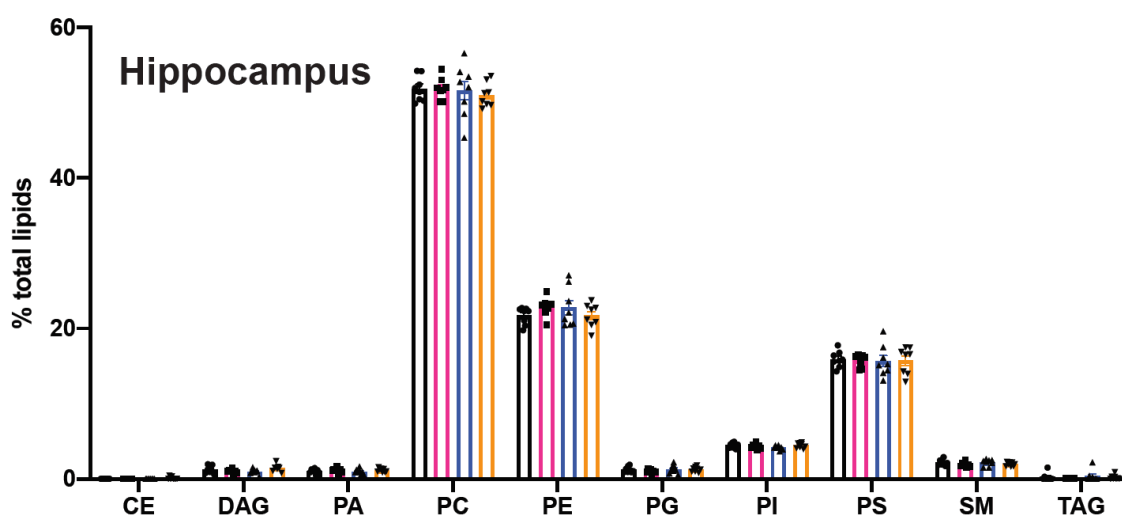
771



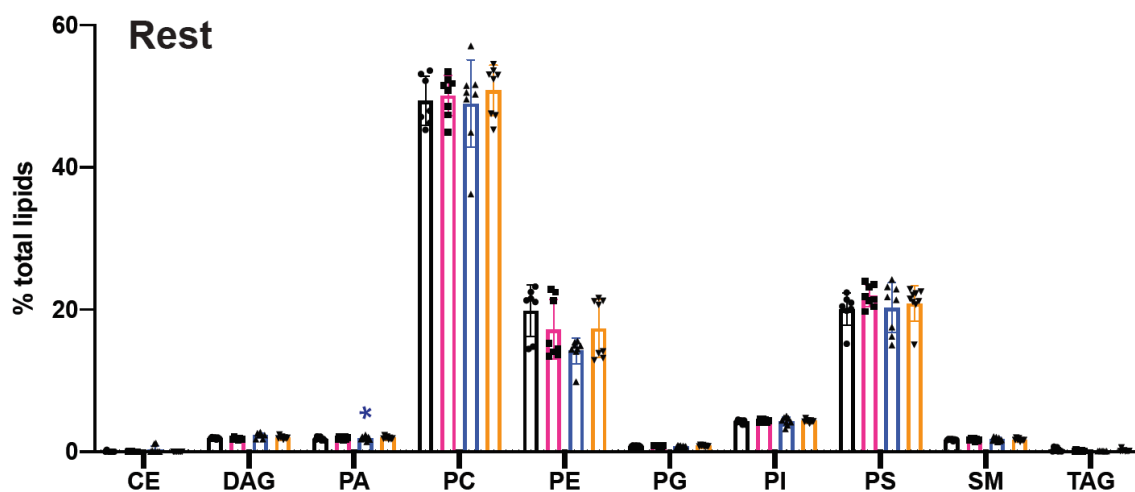
772



773



774



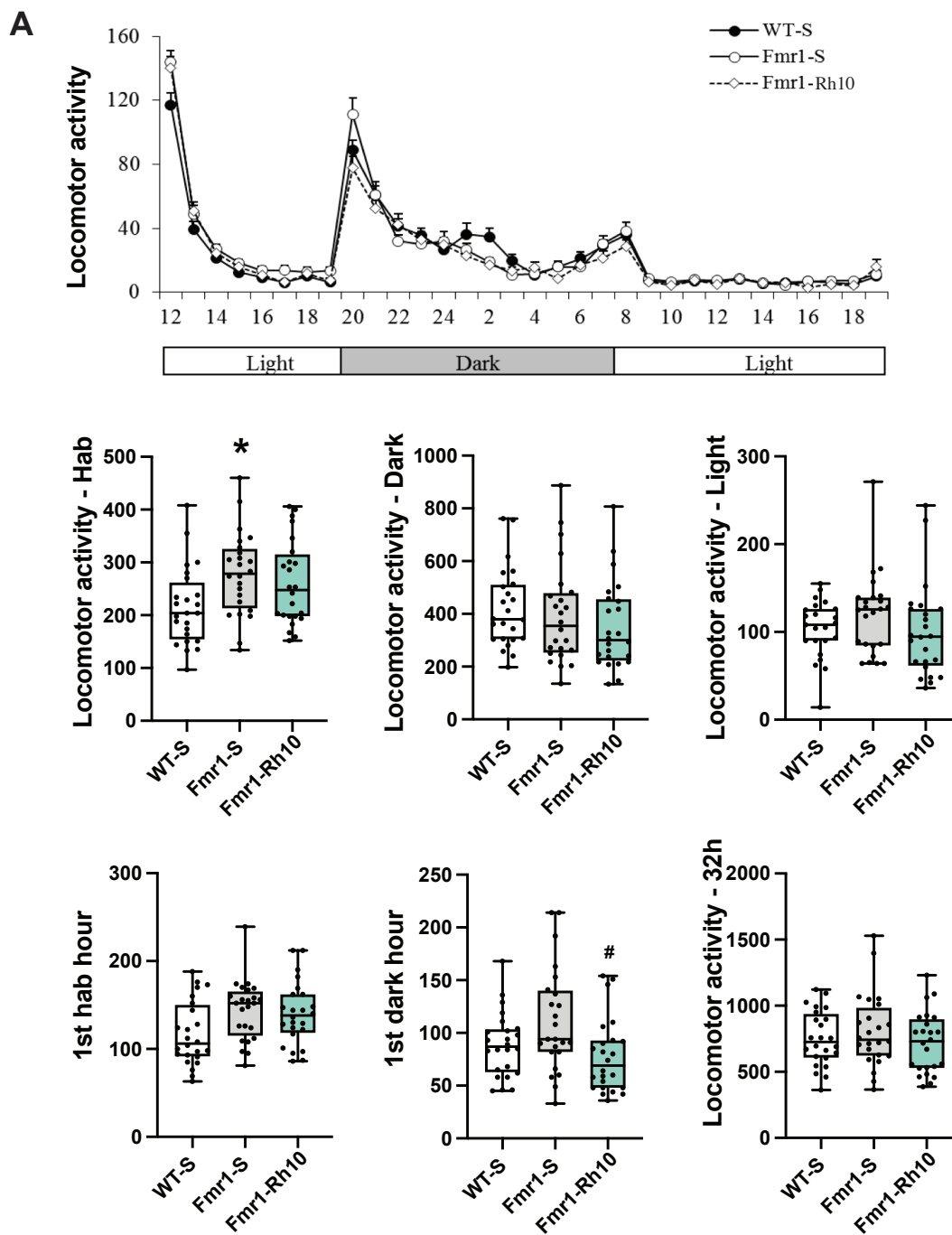
775

776

777 **Supplementary Fig. 3 : Δ N-DGKk expression in brain with AVV vectors is stable over**
778 **time and normalizes phosphatidic acid level. A)** Representative coronal brain sections
779 processed for detection of Δ N-DGKk at 8 and 12 weeks post-injections using
780 immunohistochemistry on Fmr1-KO mice treated with indicated treatment, counter stained
781 with eosin hematoxylin. Three regions a, b, c, are shown with their corresponding position on
782 brain sagittal map. Scale bar 2mm. **B)** Measure of total phosphatidic acid (PA) level by mass
783 spectrometry in hippocampus and rest of brain of WT mice treated with saline solution (WT)
784 and Fmr1-KO mice treated with saline (Fmr1-S), AAVPHP.eB- Δ N-DGKk (Fmr1-PHP.eB),
785 AAVRh10- Δ N-DGKk (Fmr1-Rh10) 8 weeks after injections. Data are expressed as mean \pm
786 SEM of mol % of total lipids and analyzed using one-way ANOVA and Tukey's multiple
787 comparisons test, * p <0.05, ** p <0.01, n =8 individual animals, except for WT n =7. **C)** Total
788 diacylglycerol (DAG) level in cortex measured as in B). PA and DAG individual species level
789 respectively in cortex (**D, G**), hippocampus (**E, H**), and rest of brain (**F, I**). **J)** lipid
790 composition (mol % of total lipid) for cholesterol esters (CE), diacylglycerol (DAG),
791 phosphatidic acid (PA), phosphatidylcholine (PC), phosphatidylethanolamine (PE),
792 phosphatidylglycerol (PG), phosphatidylinositol (PI), phosphatidylserine (PS), sphingomyelin
793 (SM), triacylglycerol (TAG), measured as in A. Data are expressed as mean \pm SEM and
794 analyzed using two-way ANOVA. * p <0.05, ** p <0.01, *** p <0.001, **** p <0.0001 vs WT-S,
795 # p <0.05, ## p <0.01, ### p <0.001, #### p <0.0001 vs Fmr1-S.

Sup Fig. 4A

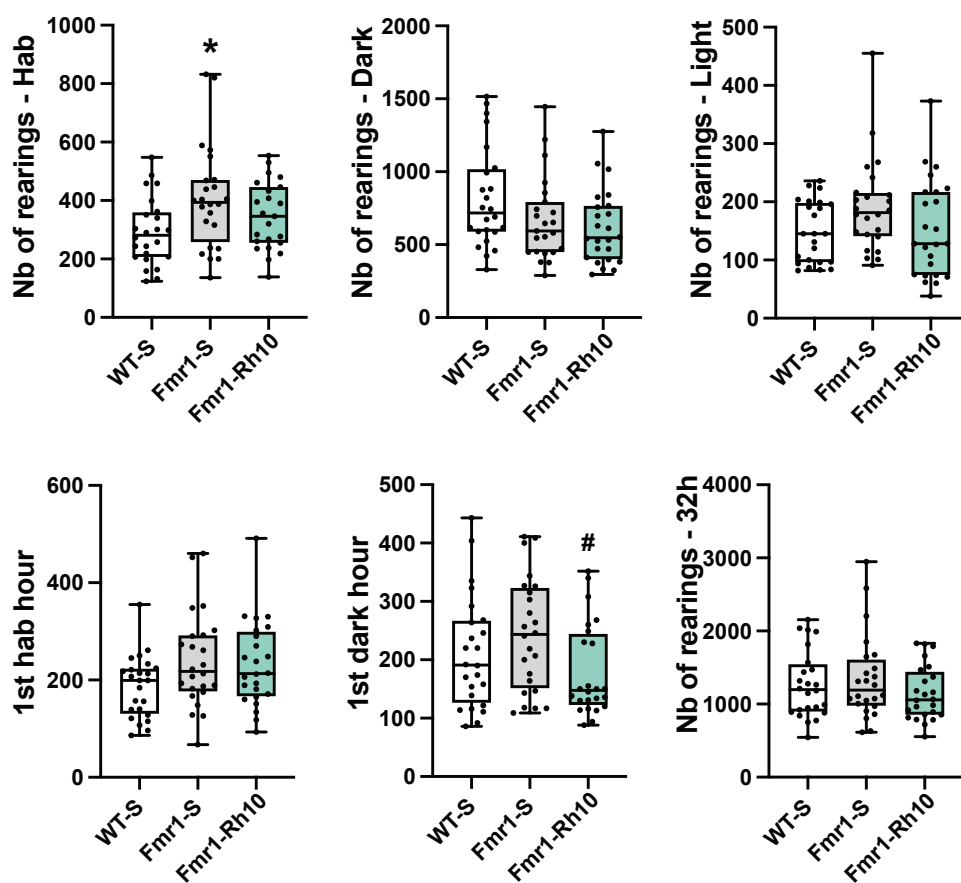
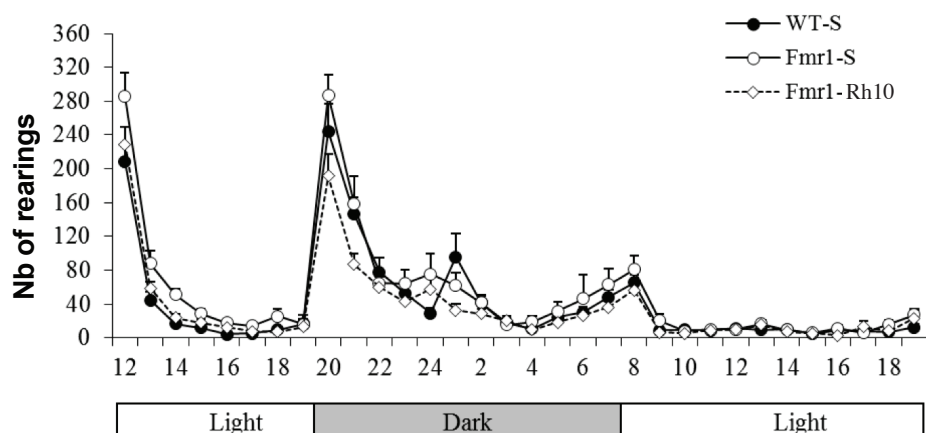
Habbas et al.



Sup Fig. 4B

Habbas et al.

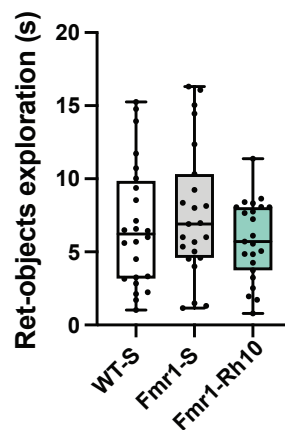
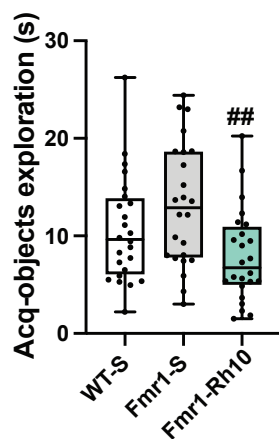
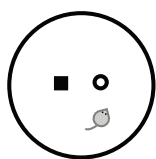
B



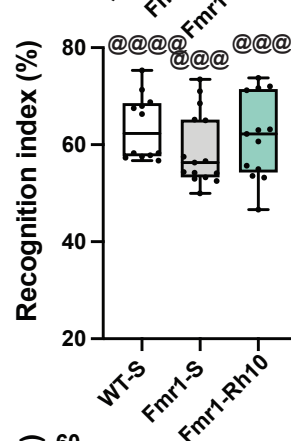
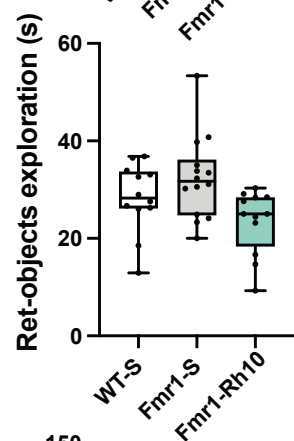
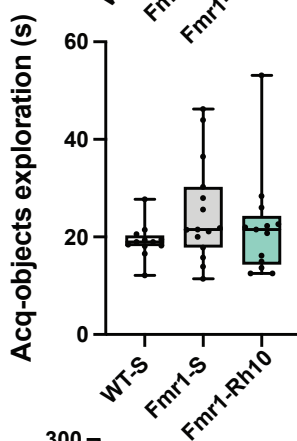
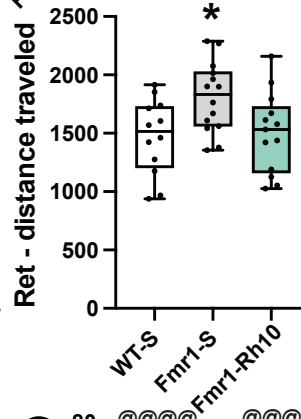
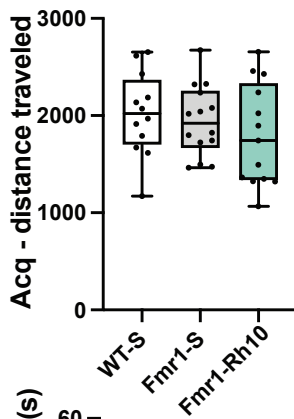
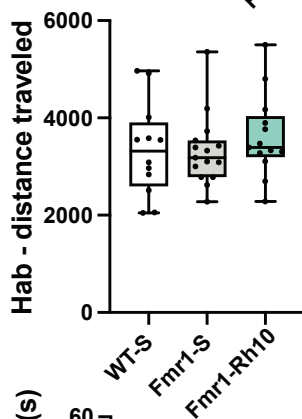
Sup Fig. 4CDE

Habbas et al.

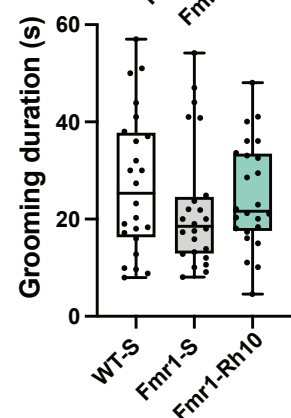
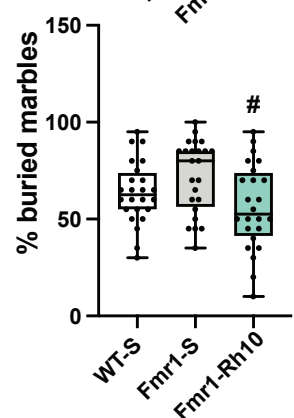
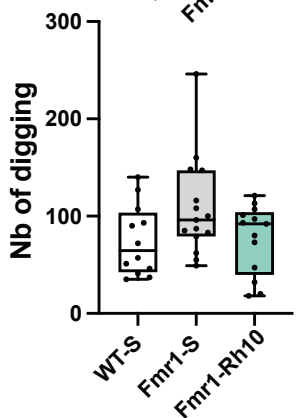
C



D



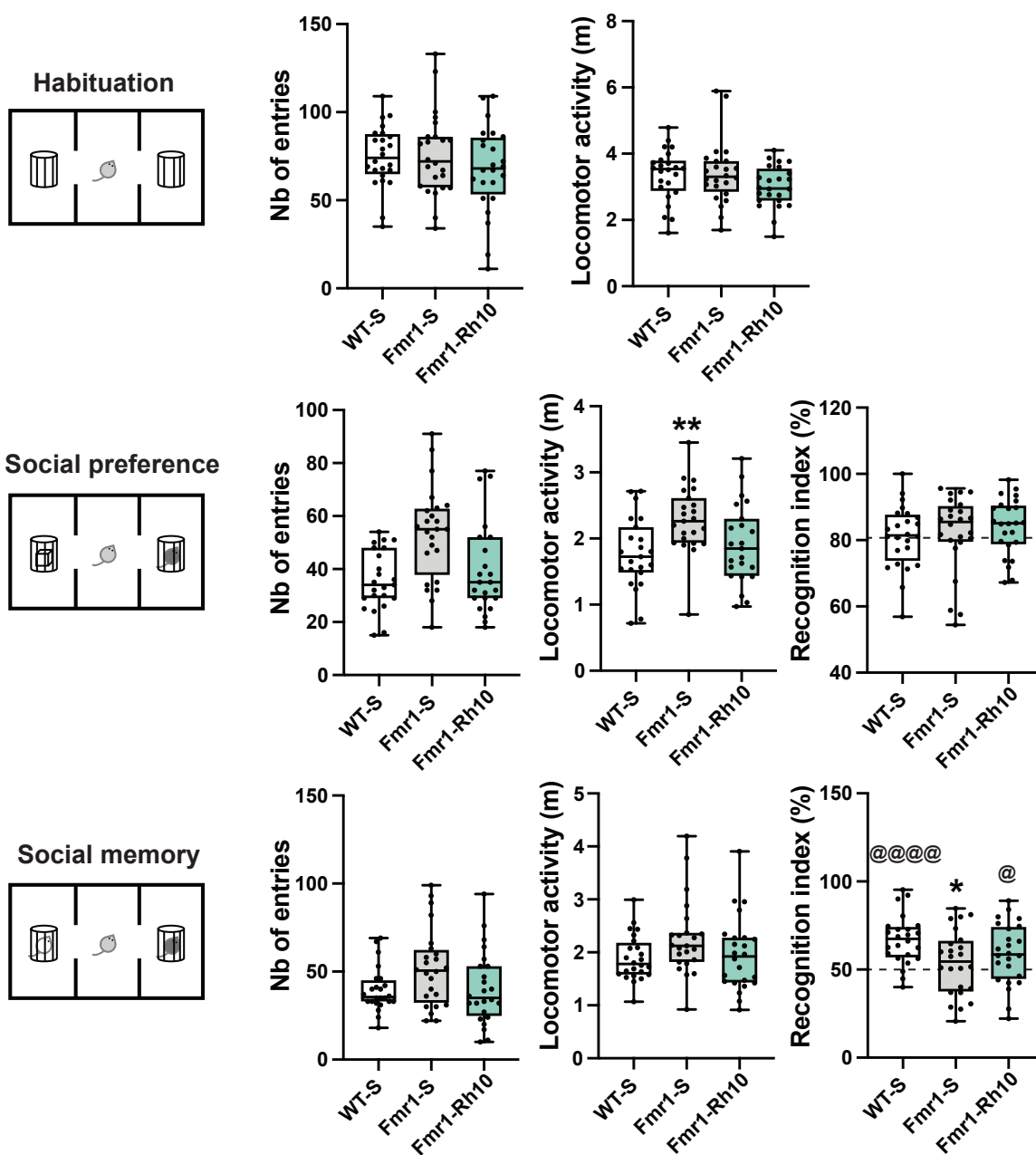
E



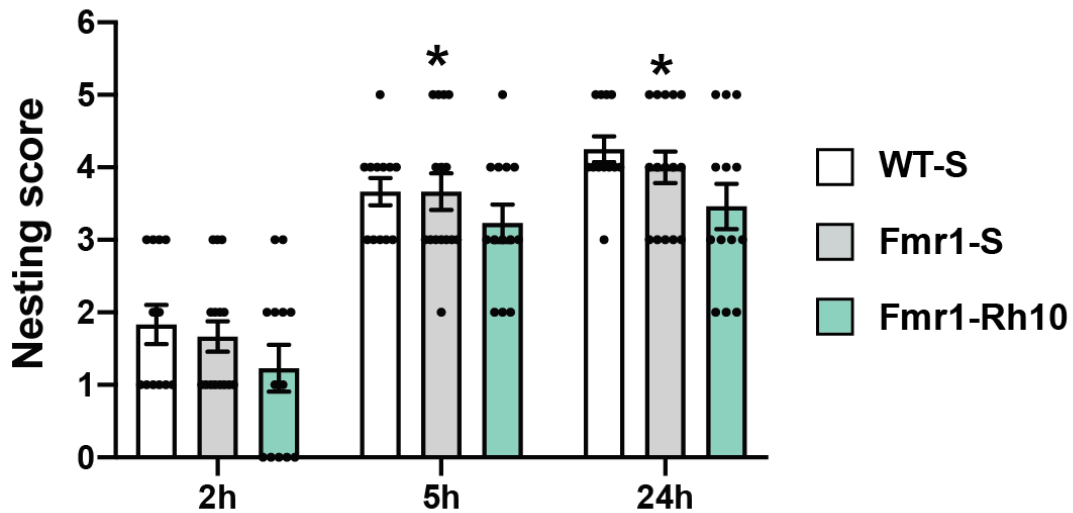
Sup Fig. 4F

Habbas et al.

F



G

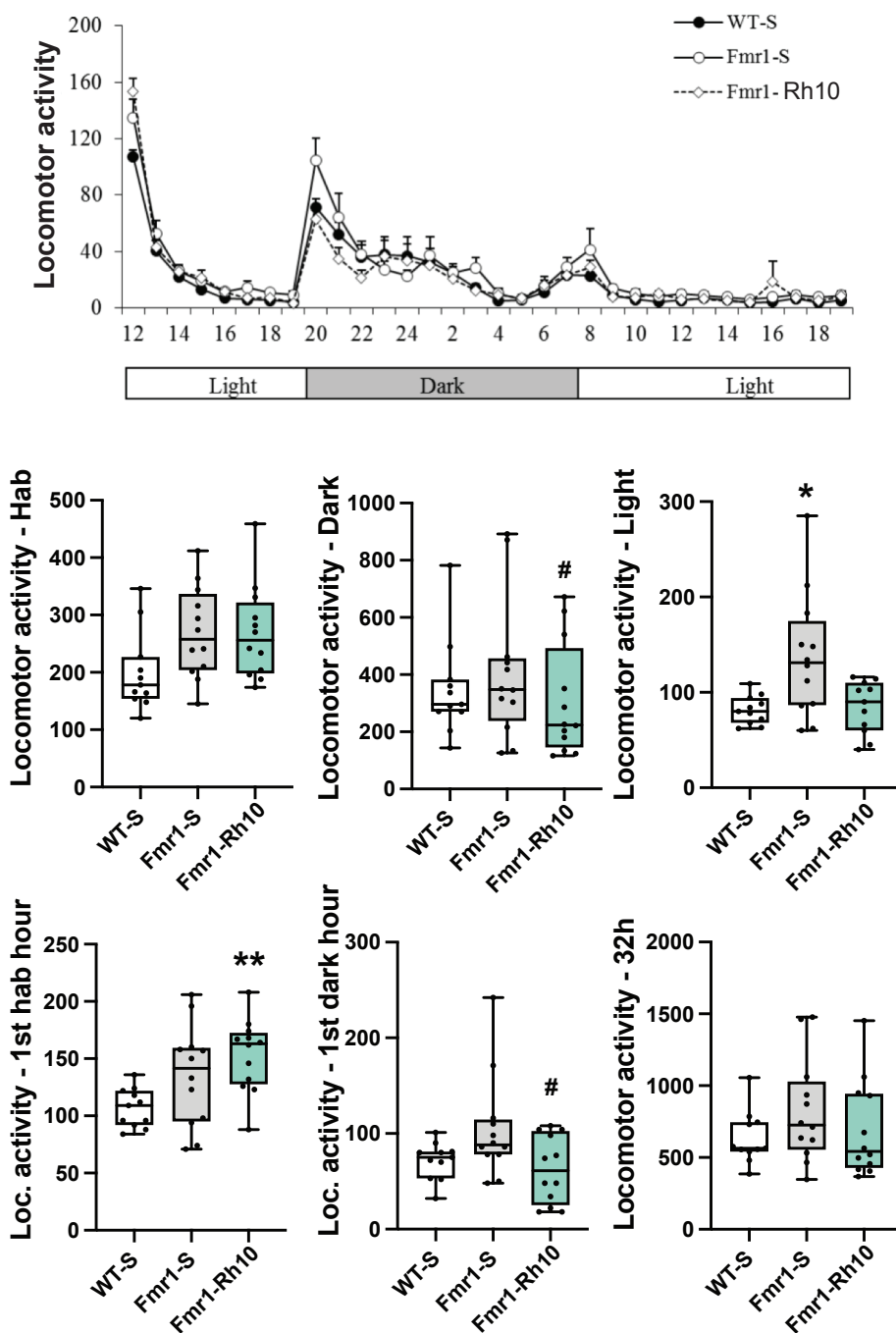


800
801 **Supplementary Fig. 4 : Behavioral analyses of AAVRh10-ΔN-DGKk treated *Fmr1*-KO**
802 **mice (4 weeks after injection).** **A)** Circadian activity (locomotor activity). Evolution of
803 locomotor activity per hour over the 32h testing (upper panel) and total locomotor activity for
804 the habituation, dark and light phases (mid panel) and for the first habituation hour, first dark
805 hour and total duration (lower panel). **B)** Circadian activity (rearing activity). Evolution of
806 rearing activity per hour over the 32h testing (upper panel) and total rearing activity for the
807 habituation, dark and light phases (mid panel) and for the first habituation hour, first dark
808 hour and total duration (lower panel). **C)** Novel object recognition in 50cm diameter arena
809 (30cm height). Duration of objects exploration during the acquisition and retention trials. **D)**
810 Novel object recognition in 30cm diameter arena (30cm height). Locomotor activity
811 (distance) in the whole arena during the 15min habituation, acquisition and retention trials.
812 Duration of objects exploration during the acquisition and retention trials and recognition
813 index. **E)** Digging, marble burying and grooming duration tests. **F)** Social recognition.
814 Number of entries and locomotor activity (total traveled distance in cm) in the two side
815 compartments during habituation (up), social preference (middle) and social memory
816 (bottom) sessions. Social preference was determined as percentage of exploration of a
817 congener vs an object (middle right) and social memory as percentage of exploration of a
818 novel vs familiar congener (bottom right). **G)** Nest building. Scoring of nests at 2, 5 and 24h.
819 0-5 scale as described by Gaskill et al (2013): 0 = undisturbed nesting material; 1 = disturbed
820 nesting material but no nest site; 2 = a flat nest without walls; 3 = a cup nest with a wall less
821 than ½ the height of a dome that would cover a mouse; 4 = an incomplete dome with a wall ½
822 the height of a dome; 5 = a complete dome with walls taller than ½ the height of a dome,
823 which may or may not fully enclose the nest. Data are expressed as median with interquartile
824 range with minimum and maximum values for A-F, mean ± SEM for G, and analyzed using
825 one-way ANOVA and Tukey's multiple comparisons test. * p<0.05 vs WT-S; # p<0.05 vs
826 *Fmr1*-S; one group t-test. *p<0.05 vs WT-S, @@@ p<0.001, @@@@ p<0.0001 vs chance
827 (50%); and χ^2 test. *p<0.05 vs WT-S.

Sup Fig. 5A

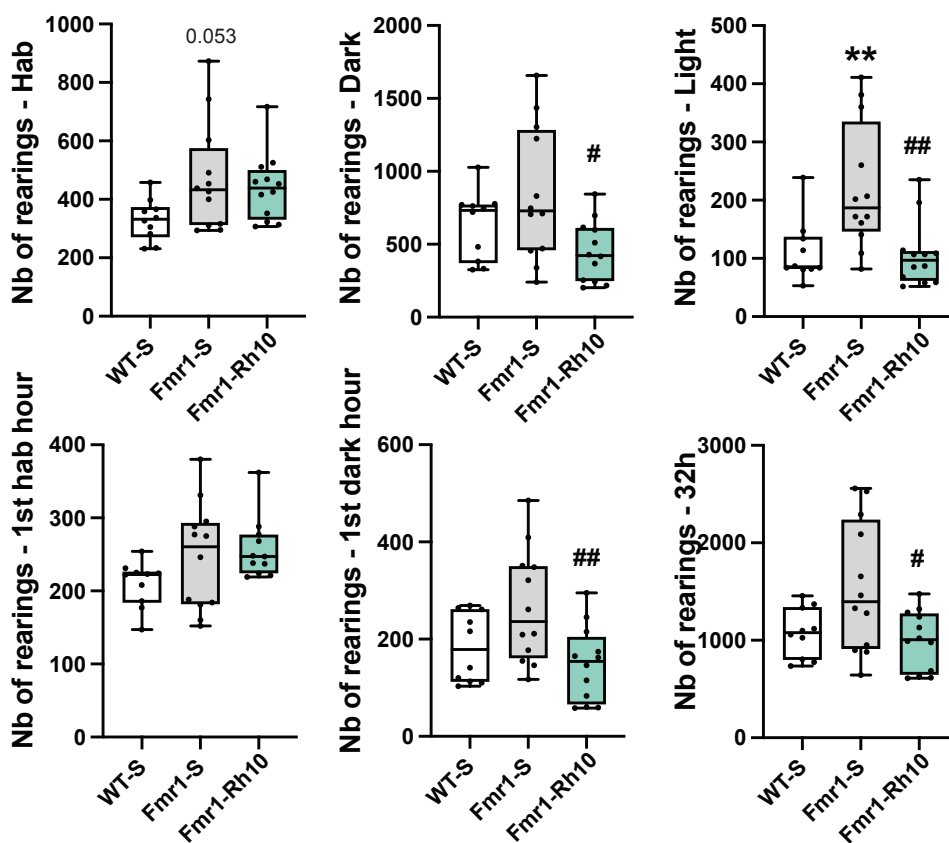
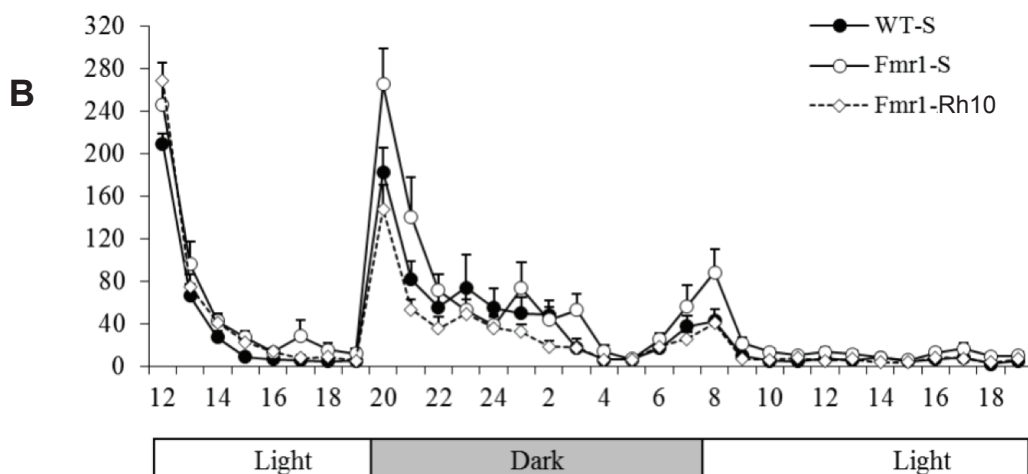
Habbas et al.

A



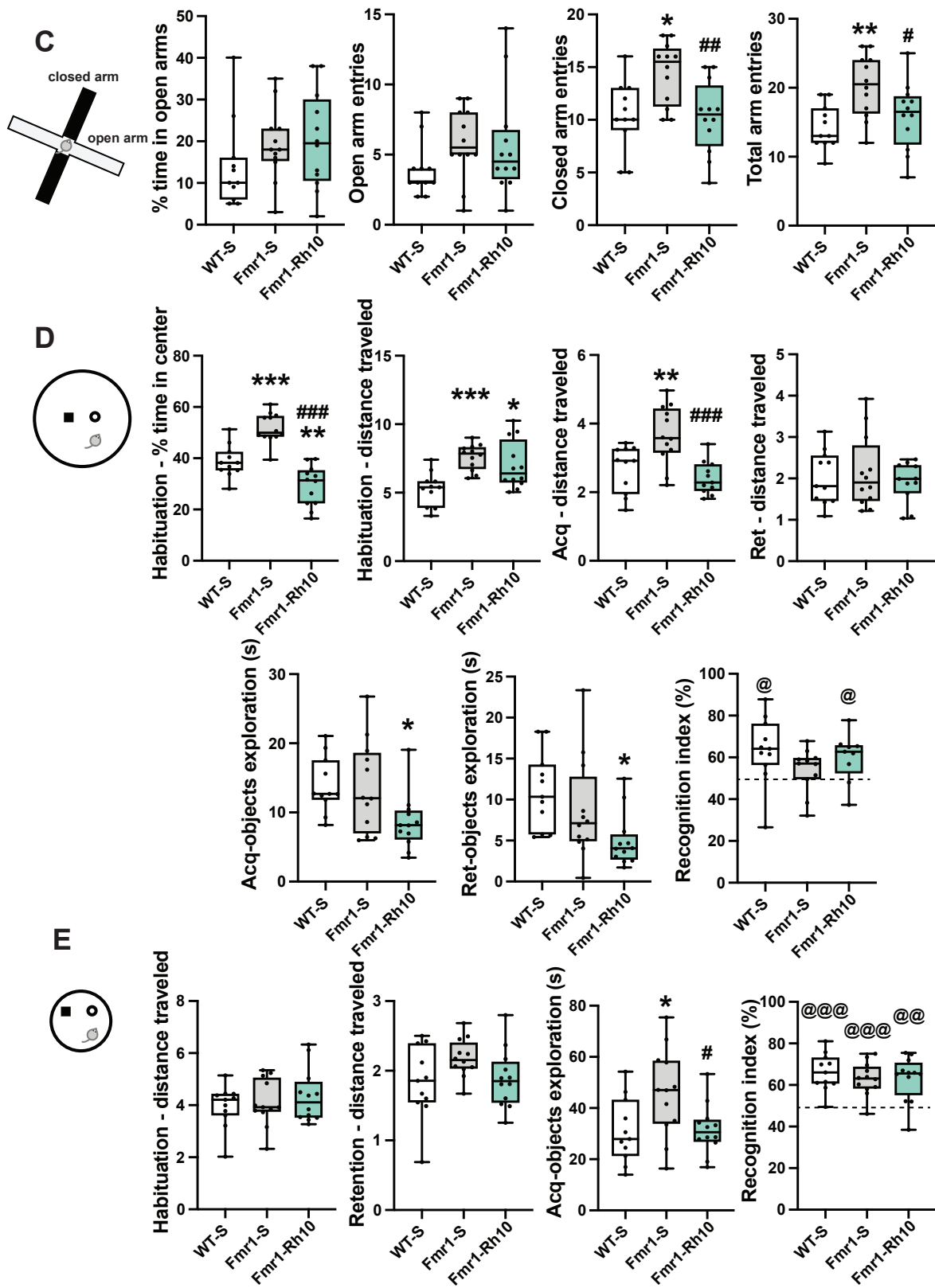
Sup Fig. 5B

Habbas et al.



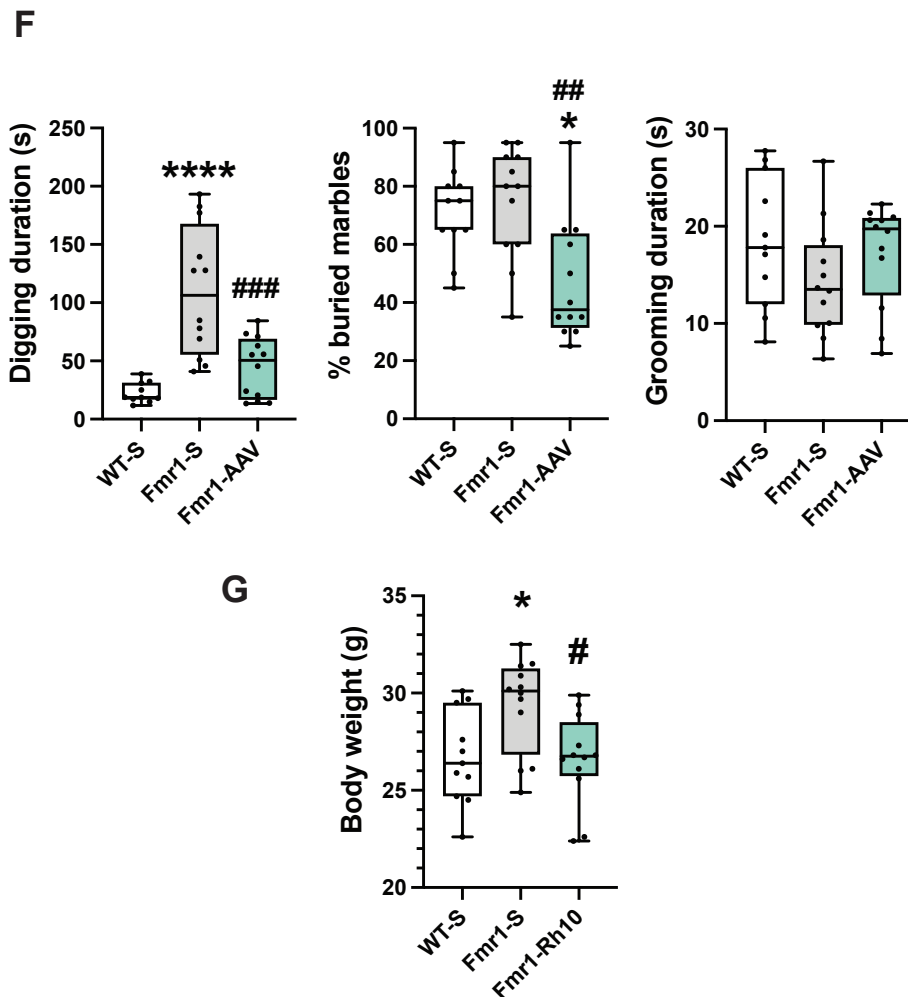
Sup Fig. 5 C-E

Habbas et al.



Sup Fig. 5 FG

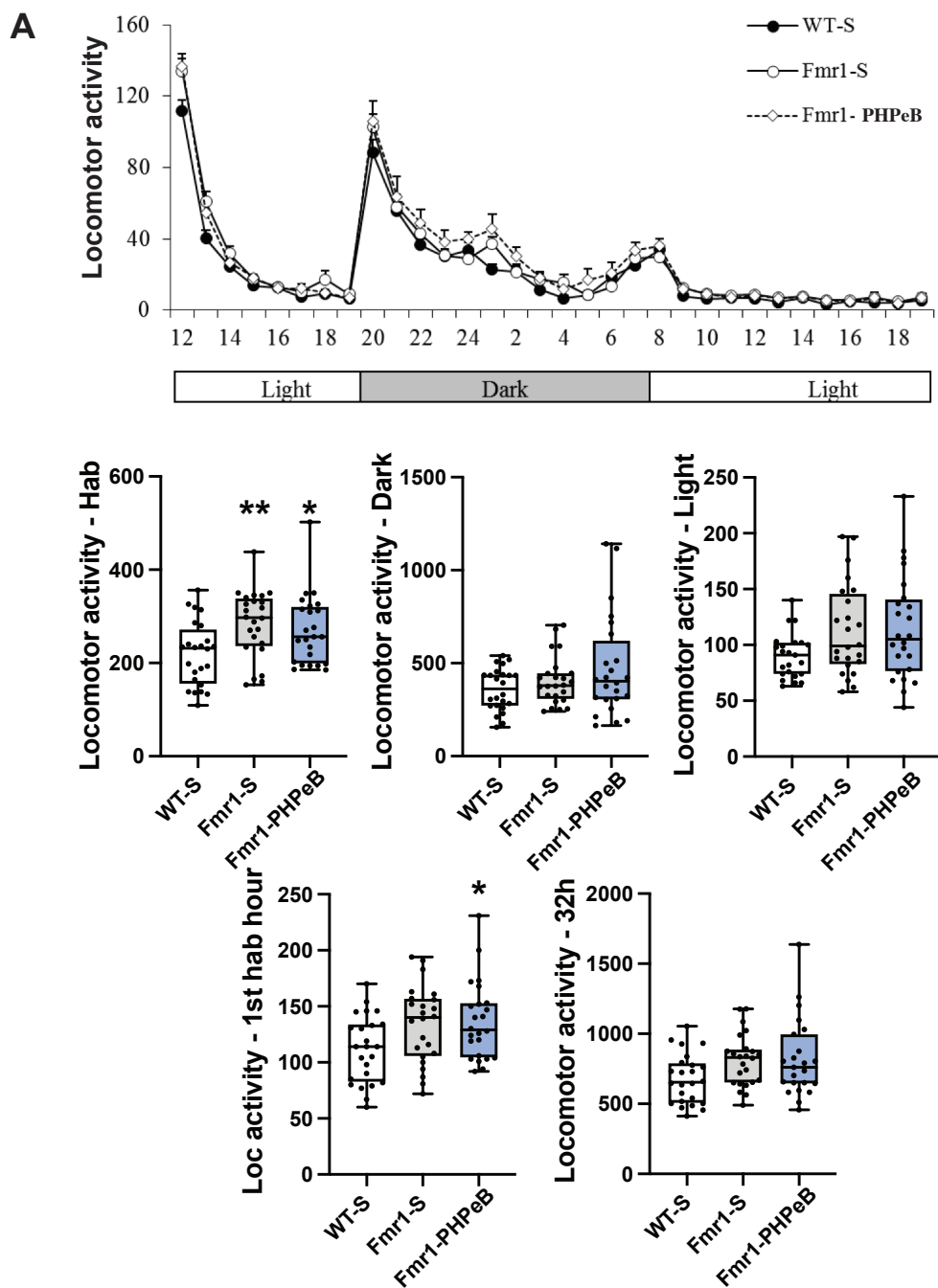
Habbas et al.



831
832 **Supplementary Fig. 5 : Behavioral analyses of AAVRh10- Δ N-DGKk treated *Fmr1*-KO**
833 **mice (8 weeks after injection).** Circadian activity analysis of locomotor (A) and rearing (B)
834 activity per hour over the 32h testing (upper panel) and total locomotor and rearing activity
835 for the habituation, dark and light phases (mid panel) and for the first habituation hour, first
836 dark hour and total duration (lower panel). C) Elevated Plus Maze. Percentage of time spent
837 in open arms and number of entries in open, closed and total (open+closed) arms. D) Novel
838 object recognition in 50cm diameter arena (30cm height). Percentage of time spent in the
839 center during the habituation, locomotor activity (distance) in the whole arena during the
840 habituation, acquisition and retention trials. Duration of objects exploration during the
841 acquisition and retention trials and recognition index. E) Novel object recognition in 30cm
842 diameter arena (30cm height). Locomotor activity (distance) in the whole arena during the
843 habituation and retention trials. Duration of objects exploration during the acquisition trials
844 and recognition index. F) Digging, marble burying and grooming duration tests. G) Body
845 weight of mice. Data are expressed as median with interquartile range with minimum and
846 maximum values and analyzed using one-way ANOVA, Tukey's multiple comparisons test
847 and one group t-test. * $p < 0.05$, ** $p < 0.01$, *** $p < 0.001$ vs WT-S, # $p < 0.05$, ## $p < 0.01$, ###
848 $p < 0.001$ vs Fmr1-S, @ $p < 0.05$, @@ $p < 0.01$, @@@ $p < 0.001$ vs chance (50%).
849

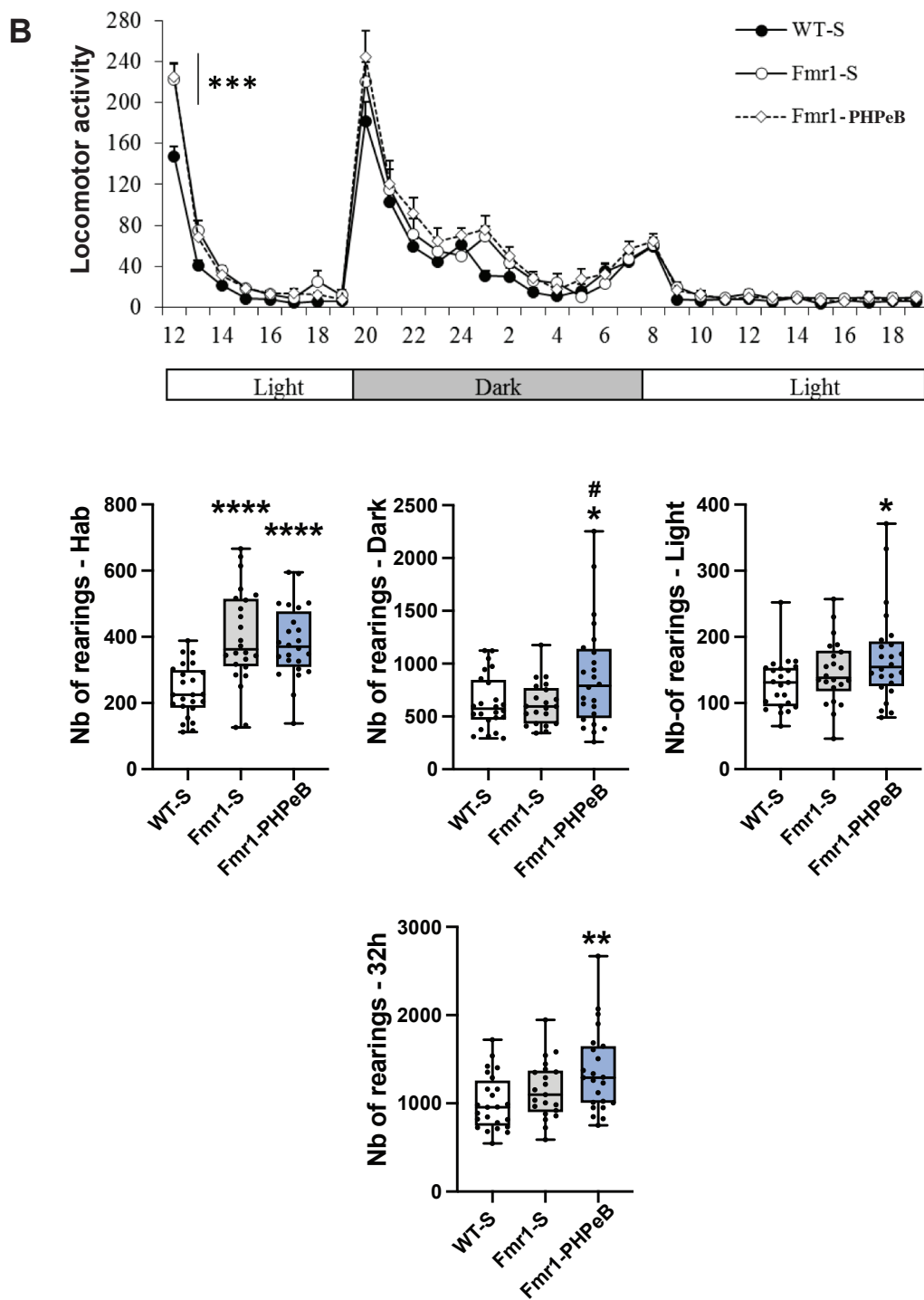
Sup Fig. 6 A

Habbas et al.



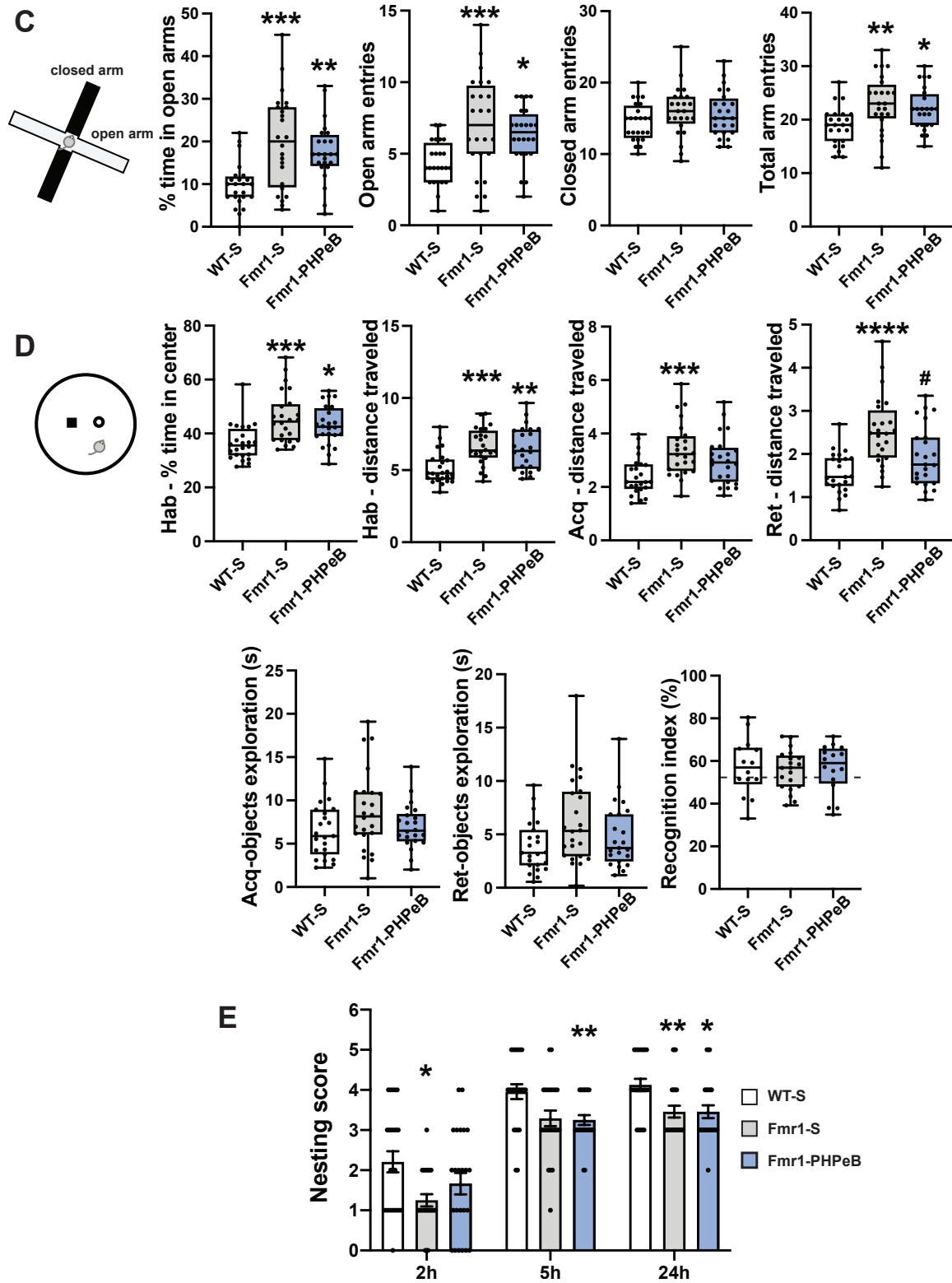
Sup Fig. 6 B

Habbas et al.



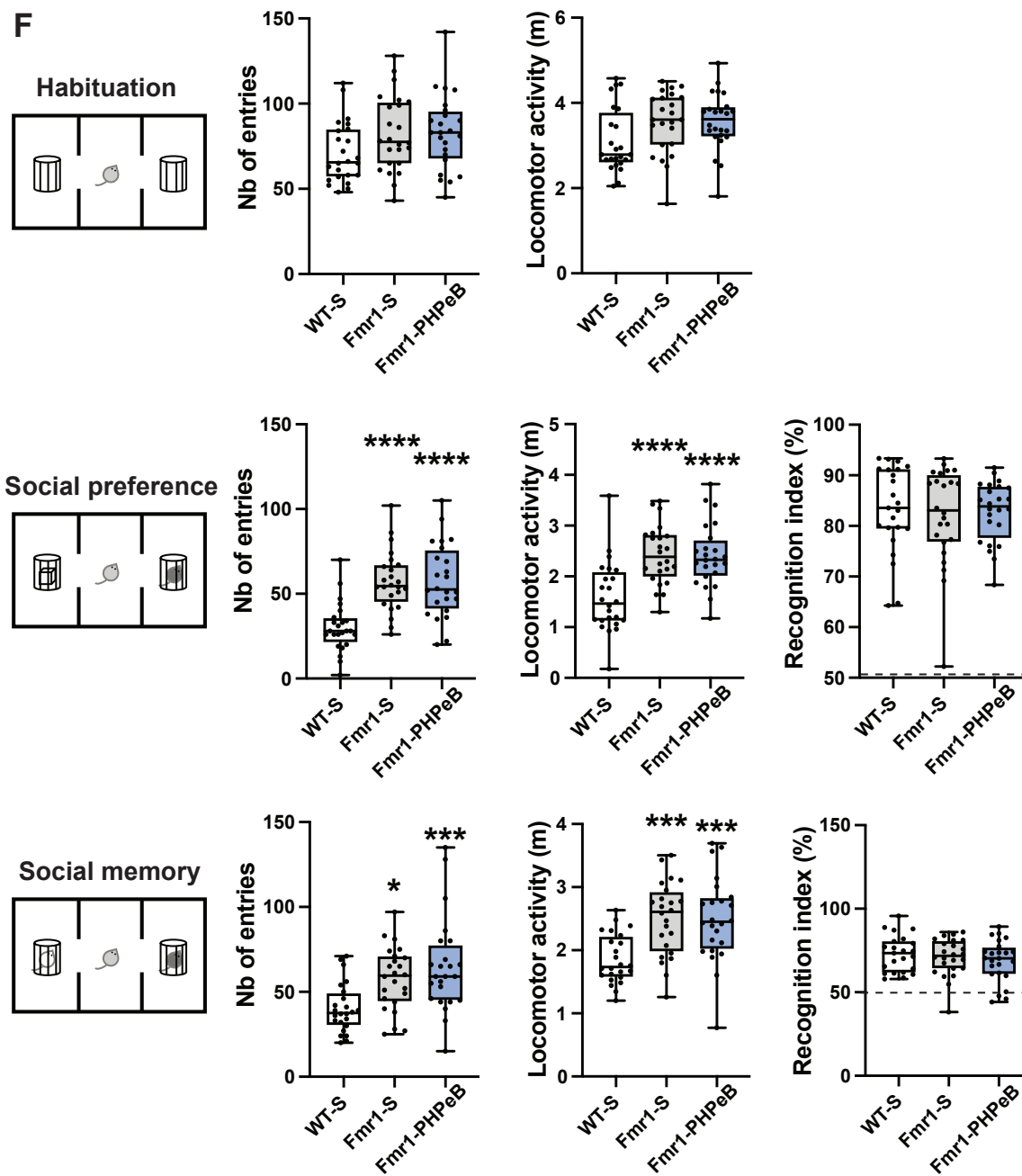
Sup Fig. 6 C-E

Habbas et al.



Sup Fig. 6 F

Habbas et al.

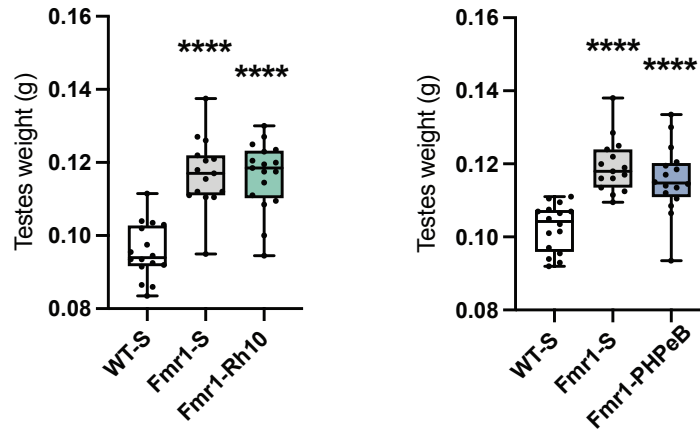


853
854

855 **Supplementary Fig. 6 : Behavioral analyses of AAVPHP.eB- Δ N-DGKk treated *Fmr1*-**
856 **KO mice (4 weeks after injection).** Circadian activity analysis of locomotor (A) and rearing
857 (B) activity per hour over the 32h testing (upper panel) and total locomotor and rearing
858 activity for the habituation, dark and light phases (mid panel) and for the first habituation
859 hour, first dark hour and total duration (lower panel). C) Elevated Plus Maze. Percentage of
860 time spent in open arms and number of entries in open, closed and total (open+closed) arms.
861 D) Novel object recognition in 50cm diameter arena (30cm height). Percentage of time spent
862 in the center during the habituation, locomotor activity (distance) in the whole arena during
863 the habituation, acquisition and retention trials. Duration of objects exploration during the
864 acquisition and retention trials and recognition index. E) Nest building. Scoring of nests at 2,
865 5 and 24h as in Sup. Fig. 4. F) Social recognition. Number of entries and locomotor activity
866 in the two side compartments during habituation (up), social preference (middle), social
867 memory (bottom) sessions. Social preference was determined as percentage of exploration of
868 a congener vs an object (middle right) and social memory as percentage of exploration of a
869 novel vs familiar congener (bottom right). Data are expressed as median with interquartile
870 range with minimum and maximum values for A-F, as mean \pm SEM for E and analyzed using
871 one-way ANOVA, Tukey's multiple comparisons test and one group t-test (recognition index)
872 or χ^2 test (nesting). * $p < 0.05$ vs WT-S. * $p < 0.05$, ** $p < 0.01$, *** $p < 0.001$, **** $p < 0.0001$ vs
873 WT-S, # $p < 0.05$ vs *Fmr1*-S.
874

Sup Fig. 7

Habbas et al.



875
876 **Supplementary Fig. 7. Testes weight of AAVRh10- Δ N-DGKk (left) and AAVPHP.eB-**
877 **Δ N-DGKk (right) treated *Fmr1*-KO mice (12 weeks after injection).** Data are means of the
878 two testes of each animal and expressed as median with interquartile range with minimum and
879 maximum values and analyzed using one-way ANOVA, Tukey's multiple comparisons test
880 *** $p < 0.0001$ vs WT-S.
881

Sup Table 1

Habbas et al.

Age (weeks): 5 6-8 9 10 11 12 13 14 15 16 →

Group 4W	Injection AAVRh10 PHPeB	Monitoring /acclimatation	Circadian activity Plus Maze	Open field Grooming	Nesting NOR Marble burying	Social Recognition				
Group 8W	Injection AAVRh10 PHPeB	Monitoring /acclimatation					Circadian activity Plus Maze	Open field Grooming	Nesting NOR Marble burying	Social Recognition

882

883 **Supplementary table 1: Phenotyping pipeline**

884

Supplementary table 2

Name of test	Rh10				PHPeB			
	4 Weeks n=24 KO vs. WT	KORH10,KO KORH10,WT	8 Weeks n=12 KO vs. WT	KORH10,KO KORH10,WT	4 Weeks n=24 KO vs. WT	KOHrPeB,KO KOHrPeB,WT	KO vs. WT	8 Weeks n=12 KOHrPeB,KO KOHrPeB,WT
Locomotor activity (cm)								
- Habitation light phase	*** increased	ns (trend to be decreases)	ns	ns	*** increased	ns	ns	ns
- Dark phase	ns	ns	ns	ns	ns	ns	ns	ns
- Light phase	ns	ns	ns	ns	ns	ns	ns	ns
- 1st Habitation H	ns, trend to be increased	ns	ns	ns	ns (trend to be increase)	ns	ns	ns
- 1st Dark hour	ns	ns	ns	ns	ns	ns	ns	ns
- 1st Dark hour - total (2h)	ns	ns	ns	ns	ns	ns	ns	ns
Rearing (nb)								
- Habitation light phase	*** increased	ns	ns (trend to be increase)	ns	*** increased	ns	ns	*** increased
- Dark phase	ns	ns	ns	ns	ns	ns	ns	ns
- Light phase	ns	ns	ns	ns	ns	ns	ns	ns
- 1st Habitation H	ns	ns	ns	ns	ns	ns	ns	ns
- 1st Dark hour	ns	ns	ns	ns	ns	ns	ns	ns
- 1st Dark hour - total (2h)	ns	ns	ns	ns	ns	ns	ns	ns
Elevated Plus maze								
% time in open arms	*** increased	ns (trend to be decreases)	ns	ns	*** increased	ns (trend to be decrease)	ns	*** increased
Open arm entries	*** increased	ns (trend to be decreases)	ns	ns	*** increased	ns (trend to be decrease)	ns	*** increased
Closed arm entries	*** increased	ns	ns	ns	*** increased	ns	ns	ns
Total arm entries	*** increased	ns	ns	ns	*** increased	ns	ns	ns
Novel Object Recognition								
- Habitation – distance traveled	*** increased	ns (trend to be decreases)	ns	ns	*** increased	ns	ns	*** increased
- Habituation – % time in center	*** increased	ns	ns	ns	*** increased	ns (trend to be decrease)	ns	*** increased
- Acquisition – distance traveled	*** increased	ns	ns	ns	*** increased	ns	ns	*** increased
- Retention – distance traveled	*** increased	ns	ns	ns	*** increased	ns	ns	*** increased
- Acquisition – exploration (s)	ns, trend to be increased	ns	ns	ns	ns	ns	ns	ns
- Retention – exploration (s)	ns	ns	ns	ns	ns	ns	ns	ns
- Retention – exploration (s)	ns	ns	ns	ns	ns	ns	ns	ns
- Recognition index (%) 50 cm arena	ns (WT vs chance)	ns (KO vs chance)	ns (KO-Hr vs chance)	ns (KO-Hr ns vs chance)	ns (WT vs chance)	ns (KO vs chance)	ns (KO-Hr ns vs chance)	ns (KO vs chance)
- Recognition index (%) 30 cm arena	ns (WT vs chance)	ns (KO vs chance)	ns (KO-Hr ns vs chance)	ns (KO-Hr ns vs chance)	ns (WT vs chance)	ns (KO vs chance)	ns (KO-Hr ns vs chance)	ns (KO vs chance)
Stereotypes								
- Marble burying (%)	ns (trend to be increased)	ns	ns	ns	ns	ns	ns	ns
- Grooming duration (s)	ns (trend to be decreases)	ns	ns	ns	ns	ns	ns	ns
- Digging (Nb)	ns	ns (trend to be decreases)	ns	ns	ns	ns	ns	ns
Nest building								
- Nesting score								
2h	trend to be decreased	ns	ns	ns	ns	ns	ns	ns
5h	*** decreased	ns	ns	ns	ns	ns	ns	ns
24h	*** decreased	ns	ns (trend to be decrease)	ns	ns	ns	ns	ns
Social Memory								
- Habituation – Nb entries	ns	ns	ns (trend to be increase)	ns	ns	ns (trend to be increase)	ns	ns
- Habituation – distance traveled (cm)	ns	ns	ns	ns	ns	ns	ns	ns
- Social preference – Nb entries	*** increased	ns	ns	ns	*** increased	ns	ns	ns
- Social preference – distance traveled	*** increased	ns (trend to be decreases)	ns	ns	*** increased	ns	ns	ns
- Social memory – Nb entries	ns (trend to be increased)	ns (trend to be decreases)	ns	ns	ns	ns	ns	ns
- Social memory – distance traveled	ns	ns	ns	ns	ns	ns	ns	ns
- Social preference – sniffing duration	ns (WT vs chance)	ns (KO vs chance)	ns (KO-Hr ns vs chance)	ns (KO-Hr ns vs chance)	ns (WT vs chance)	ns (KO vs chance)	ns (KO-Hr ns vs chance)	ns (KO vs chance)
- Social preference – sniffing duration	ns (WT vs chance)	ns (KO vs chance)	ns (KO-Hr ns vs chance)	ns (KO-Hr ns vs chance)	ns (WT vs chance)	ns (KO vs chance)	ns (KO-Hr ns vs chance)	ns (KO vs chance)
- Social memory – sniffing duration	ns (WT vs chance)	ns (KO vs chance)	ns (KO-Hr ns vs chance)	ns (KO-Hr ns vs chance)	ns (WT vs chance)	ns (KO vs chance)	ns (KO-Hr ns vs chance)	ns (KO vs chance)
Body weight								
Weight	ns	ns	ns	ns	ns	ns	ns	ns

type of test

locomotor activity

other types of activity

memory

weight

886 **Supplementary table 2: Summary of the phenotypic comparisons between WT mice**
887 **treated saline (WT-S), *Fmr1*-KO treated saline (KO-S) and *Fmr1*-KO treated AAV**
888 **(KO-Rh10 or KO-PhPeB) 4 and 8 weeks post-treatment. *, **, ***, **** p<0.05, 0,01,**
889 **0,001, 0,0001 KO-S vs WT-S, or KO-AAV vs WT-S. #, ##, ###, #### p<0.05, 0,01, 0,001,**
890 **0,0001 KO-AAV vs KO. *p<0.05, **p<0.01, ***p<0.001, ****p<0.0001 vs WT-S, # p<0.05**
891 **vs *Fmr1*-S.**
892